

Methods and results of the IGEC search for burst gravitational waves in the years 1997–2000

P. Astone,¹ D. Babusci,² L. Baggio,^{3,4} M. Bassan,^{5,6} D. G. Blair,⁷ M. Bonaldi,^{8,4} P. Bonifazi,^{9,1} D. Busby,¹⁰ P. Carelli,¹¹ M. Cerdonio,^{12,13} E. Coccia,^{5,6} L. Conti,^{12,13} C. Cosmelli,^{14,1} S. D'Antonio,² V. Fafone,² P. Falferi,^{8,4} P. Fortini,^{15,16} S. Frasca,^{14,1} G. Giordano,² W. O. Hamilton,¹⁰ I. S. Heng,^{10,*} E. N. Ivanov,⁷ W. W. Johnson,¹⁰ A. Marini,² E. Mauceli,¹⁷ M. P. McHugh,¹⁸ R. Mezzena,^{3,4} Y. Minenkov,⁶ I. Modena,^{5,6} G. Modestino,² A. Moleti,^{5,6} A. Ortolan,¹⁹ G. V. Pallottino,^{14,1} G. Pizzella,^{5,2} G. A. Prodi,^{3,4,†} L. Quintieri,² A. Rocchi,⁵ E. Rocco,³ F. Ronga,² F. Salemi,¹⁵ G. Santostasi,¹⁰ L. Taffarello,¹³ R. Terenzi,⁹ M. E. Tobar,⁷ G. Torrioli,²⁰ G. Vedovato,¹⁹ A. Vinante,^{3,4} M. Visco,^{9,6} S. Vitale,^{3,4} and J. P. Zendri¹³

(International Gravitational Event Collaboration)

¹*Istituto Nazionale di Fisica Nucleare, Sezione di Roma 1, P. le A. Moro 2, I-00185, Roma, Italy*²*Laboratori Nazionali di Frascati, Istituto Nazionale di Fisica Nucleare, Via E. Fermi 40, I-00044, Frascati, Italy*³*Dipartimento di Fisica, Università di Trento, I-38050 Povo, Trento, Italy*⁴*Istituto Nazionale di Fisica Nucleare, Gruppo Collegato di Trento, Sezione di Padova, I-38050 Povo, Trento, Italy*⁵*Dipartimento di Fisica, Università di Roma "Tor Vergata," Via Ricerca Scientifica 1, I-00133 Roma, Italy*⁶*Istituto Nazionale di Fisica Nucleare, Sezione di Roma Due, Via Ricerca Scientifica 1, I-00133 Roma, Italy*⁷*Department of Physics, University of Western Australia, Nedlands, WA 6907 Australia*⁸*Centro di Fisica degli Stati Aggregati, IFN-CNR, Trento, I-38050 Povo, Trento, Italy*⁹*Istituto Fisica Spazio Interplanetario, CNR, Via Fosso del Cavaliere, I-00133 Roma, Italy*¹⁰*Department of Physics and Astronomy, Louisiana State University, Baton Rouge, Louisiana 70803, USA*¹¹*Dipartimento di Fisica, Università de L'Aquila, and INFN, L'Aquila, Italy*¹²*Dipartimento di Fisica, Università di Padova, Via Marzolo 8, 35131 Padova, Italy*¹³*Istituto Nazionale di Fisica Nucleare, Sezione di Padova, Via Marzolo 8, 35131 Padova, Italy*¹⁴*Dipartimento di Fisica, Università di Roma "La Sapienza," P. le A. Moro 2, I-00185, Roma, Italy*¹⁵*Dipartimento di Fisica, Università di Ferrara, I-44100 Ferrara, Italy*¹⁶*Istituto Nazionale di Fisica Nucleare, Sezione di Ferrara, I-44100 Ferrara, Italy*¹⁷*Whitehead Institute, MIT, Cambridge, Massachusetts 02142, USA*¹⁸*Department of Physics, Loyola University, New Orleans, Louisiana 70118, USA*¹⁹*Laboratori Nazionali di Legnaro, Istituto Nazionale di Fisica Nucleare, 35020 Legnaro, Padova, Italy*²⁰*Istituto Elettronica Stato Solido, IFN-CNR, Via Cineto Romano 42, Roma, Italy*

(Received 21 February 2003; published 11 July 2003)

This paper presents the results of the observations of the detectors participating in the International Gravitational Event Collaboration (IGEC) from 1997 to 2000 and reviews the data analysis methods. The analysis is designed to search for coincident excitations in multiple detectors. The data set analyzed in this article covers a longer period and is more complete than that given in previous reports. The current analysis is more accurate for determining the false dismissal probability for a time coincidence search and it optimizes the search with respect to a target amplitude and direction of the signal. The statistics of the accidental coincidences agrees with the model used for drawing the results. The observations of this IGEC search are consistent with no detection of gravitational wave burst events. A new conservative upper limit has been set on the rate of gravitational wave bursts with a Fourier component $H > 2 \times 10^{-21} \text{ Hz}^{-1}$, both for searches with and without a filter for the galactic center direction. This study confirms that the false alarm rate of the observation can be negligible when at least three detectors are operating simultaneously.

DOI: 10.1103/PhysRevD.68.022001

PACS number(s): 04.80.Nn, 95.85.Sz

I. INTRODUCTION

This paper presents the results of the observations of the International Gravitational Event Collaboration (IGEC) from 1997 to 2000. We have made an extensive search for burst-type gravitational waves with the largest network of detectors ever assembled, and report here the details of the search

and the new upper limits achieved for the rate of gravitational wave burst events.

The search for gravitational waves (GWs) involves detecting the presence of a signal in the noise of the detector array. A signal must compete with the intrinsic noise of the detectors and also with transient excitations (of mechanical or electromagnetic origin for example) which usually cannot be discriminated from the actual GW signal. Therefore, it is not viable to perform burst GW searches with a single detector. With two or more detectors in simultaneous observation, the impact of local transient excitations on burst GW searches is significantly reduced. Moreover, the false alarm

*Presently at Max-Planck-Inst. für Gravitationsphysik, Albert-Einstein-Inst. Hannover, Callinstr. 38, 30167 Hannover, Germany.

†Corresponding author. Email address: prodi@science.unitn.it

TABLE I. Summary of detector characteristics. The reported misalignment is the angle between the bar axis and a common direction. The observation time refers to the data exchanged for this 1997–2000 IGEC analysis.

Detector	ALLEGRO	AURIGA	EXPLORER	NAUTILUS	NIOBE
Material	Al5056	Al5056	Al5056	Al5056	Nb
Mass [kg]	2296	2230	2270	2260	1500
Length [m]	3.0	2.9	3.0	3.0	2.8
Resonant frequencies [Hz]	920	930	921	924	713
	895	912	905	908	694
Temperature [K]	4.2	0.2	2.6	0.1	5.0
Longitude	268°50'E	11°56'54"E	6°12'E	12°40'21"E	115°49'E
Latitude	30°27'N	45°21'12"N	46°27'N	41°49'26"N	−31°56N
Azimuth	40°W	44°E	39°E	44°E	0°
Misalignment [deg]	9	4	2	3	29
Observation time [d]	852.5	216.5	551.0	414.8	192.6

rate can be reliably estimated. Hence, to facilitate multidetector searches for burst GWs the IGEC was formed in 1997.¹ This collaboration currently consists of five cryogenic resonant-bar gravitational wave detectors, ALLEGRO [1], AURIGA [2], EXPLORER [3], NAUTILUS [4], and NIOBE [5], operating as a worldwide network. The members of this network exchange lists of candidate GW events and related information under an agreed data exchange protocol.

The target signals are transients without structure in the frequency range investigated. Examples of such signals are short pulses of ~ 1 ms duration, signals showing a few cycles of ~ 1 ms period and signals sweeping in frequency across ~ 1 kHz. Possible sources are therefore related to compact astrophysical objects, such as the coalescence of neutron star and black hole binaries [6,7].

The main method used to search for burst GWs has been to search for an excess of coincident excitations in two detectors [8–11]. The IGEC performed the first thorough search on more than two detectors on data acquired in 1997 and 1998 [12]. No claims of detection were made, but an improved upper limit on burst GWs was set. In 2001 all the data acquired by IGEC members between 1997 and 2000 were exchanged. A preliminary search was performed on these data [13].

In this article, we present the results of a comprehensive search by the IGEC for burst gravitational waves on the full data set. In addition to the extended observation time, this analysis makes significant progress over the previous searches in the following respects: (i) different search thresholds are systematically tried, (ii) the time coincidence window is determined by the desired confidence level, (iii) a directional search strategy is implemented, (iv) the statistics of the estimated false alarms is thoroughly investigated, and (v) the statistical methods chosen to set the confidence inter-

vals ensure a given *coverage*,² i.e., the probability that the confidence interval contains the true value. In the following section, we review the IGEC operation during 1997–2000. The methods of the multidetector analysis are described in Sec. III. Finally, in Sec. IV, we discuss the results. In this section we pay particular attention to the new upper limit on the rate of detected burst GWs³ and on the low level of false alarms achieved by this observatory.

II. EXCHANGED DATA

In this section we review the 1997–2000 operation of the IGEC. We recall the sensitivity to burst GWs of the participating bar detectors (see Sec. II A). Each detector group searches its data independently for *gravitational wave candidates* or *events*. Then, the information exchanged under the IGEC is described, with particular attention to the data validation requirements (see Sec. II B). The quality of the contribution of each detector to the IGEC observatory is discussed in terms of observation time and false alarms as a function of a threshold on the amplitude of target GW signals (see Sec. II C). The statistics of the time series of the exchanged events shows autocorrelation at short time scales. This clustering, however, disappears when cross-correlating different detectors (see Sec. II D).

²In this analysis, we refer to the conventional frequentist *coverage*, i.e., the probability that the confidence interval contains the true GW value. In other words, the coverage is the probability as could be measured in principle by repeating the same observations with the same GW source, where “same” is meant in the stochastic sense. In this analysis, we made conservative estimates of the coverage.

³The authors Astone, Pallottino and Pizzella point out that the analysis presented in this paper is aimed at a systematic search for coincident excitations in multiple detectors; however, they are convinced that a probabilistic estimation of the flux of GWs on Earth as well as of upper limits requires a Bayesian approach.

¹<http://igec.lnl.infn.it>

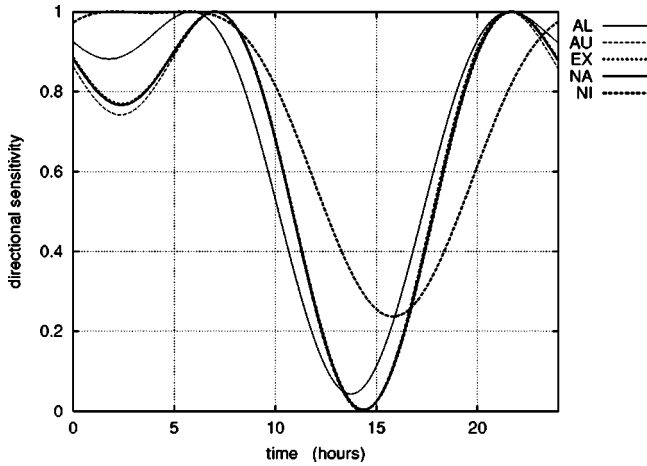


FIG. 1. Amplitude directional sensitivity of the detectors versus UTC with respect to the galactic center for DAY 25 Dec. 2000.

A. Detectors

All of the currently operating resonant detectors measure the tidal strain of a mechanically isolated cylindrical bar caused by impinging GWs. A lighter mechanical resonator is strongly coupled and tuned to the fundamental longitudinal mode of the bar, resulting in a system with two normal modes of vibration.

A list of the main characteristics of the detectors is shown in Table I. All the bars are cooled to cryogenic temperatures. AURIGA and NAUTILUS operate at a few hundred mK to further reduce contributions from the thermal noise. For the same reason, niobium was chosen as the material for NIOBE because it has a higher mechanical quality factor at 4 K.

The IGEC search is focused on burst GWs, which can be modeled as a pure Dirac δ -function excitation. The strength of a burst can be quantified by its Fourier amplitude H , or *amplitude*, which is related to the energy E_s deposited in the bar by

$$H = \frac{1}{4L\nu_0^2} \sqrt{\frac{E_s}{M}} \quad (1)$$

where L is the bar length, M its mass, and ν_0 the mean resonant frequency of the detector.

Actually, the class of detectable signals is much wider than δ functions. This search is also effective for all short duration signals which have an almost constant value for their Fourier amplitude at the detector frequencies, i.e., ~ 700 Hz for NIOBE and ~ 900 Hz for the other detectors (see Table I). In these cases, the GW amplitude H is estimated without bias.

The detectors were oriented to be nearly parallel to each other. This was done by orienting them to be perpendicular to a common great circle that passes through or near the sites. This makes their antenna patterns coherent and maximizes the probability of coincident signal detection between multiple detectors.

For cylindrical bar detectors, the amplitude observed for a GW signal from a particular source in the sky follows a $\sin^2 \theta$ function, where θ is the angle between the long axis of

the bar and the direction of the source. As a demonstration of the effectiveness of the chosen common orientation, we plot in Fig. 1 the directional sensitivity with respect to the galactic center for the five detectors of the IGEC. The sensitivity to wave polarization is then $\cos 2\psi$, where ψ is the polarization angle in the wavefront plane with respect to the projection of the bar axis.

B. IGEC data exchange protocol

Each group implements independently a burst GW search by using an optimal filter [14], which takes into account the slow variations of the noise characteristics of the detector [1,15,16]. The filter estimates the Fourier amplitude of the burst GW. An adaptive threshold, the *exchange threshold*, is then applied to the filtered data and a list of the *candidate events* above threshold is compiled.⁴ The exchange threshold is typically set to an amplitude signal-to-noise ratio (SNR) of between 3 and 5. The candidate events are described by the peak amplitude of the optimal filter output, the time of its occurrence, and the uncertainties in amplitude and time.

The IGEC protocol requires each detector to report all time intervals of satisfactory operation. This is accomplished by vetoing periods corresponding to times of laboratory activity which are known to affect the sensitivity of the detector, such as periods of cryogenic maintenance. In the case of EXPLORER and NAUTILUS, times were also vetoed when the noise variance exceeded a certain value. For AURIGA, times were vetoed when either the statistics of the noise was not Gaussian or the Wiener filter was not properly matched to the noise [17,18].

All this information is exchanged within IGEC under a common data format. This protocol was last updated in 2000 (see footnote 1). The most relevant additions introduced by that update were (i) the absence of any biases in the estimates of the time of arrival (ETA) and *amplitude* (see footnote 4), (ii) an estimate of the errors in the ETA, (iii) an upper bound of the systematic errors in amplitude, and (iv) a continuous measurement of the noise level and a continuous record of the chosen exchange threshold (i.e., the threshold used to compile the event list). The noise level is described by the standard deviation and by the third and fourth order moments of the noise distribution.

The choice of the most suitable exchange threshold is left to each group, provided that two constraints are met. One lower bound on the exchange threshold comes from the requirement of having unbiased estimates of the amplitude and ETA of the exchanged events. The other constraint is a specified criterion that limits the rate of exchanged events and

⁴The time of arrival of the impulsive excitations is not known; therefore, the optimal filter is applied continuously. The local maxima in the absolute value of the filtered output are compared to the threshold, and any maxima above are defined as candidate events. This modification of the Wiener theory introduces some nonlinearity of the estimates. The resulting bias on the amplitude and time of arrival the events has to be taken into account. In the limit of high SNR events, linearity is recovered. See, for instance, Ref. [18] for a discussion on the biases introduced at low SNR.

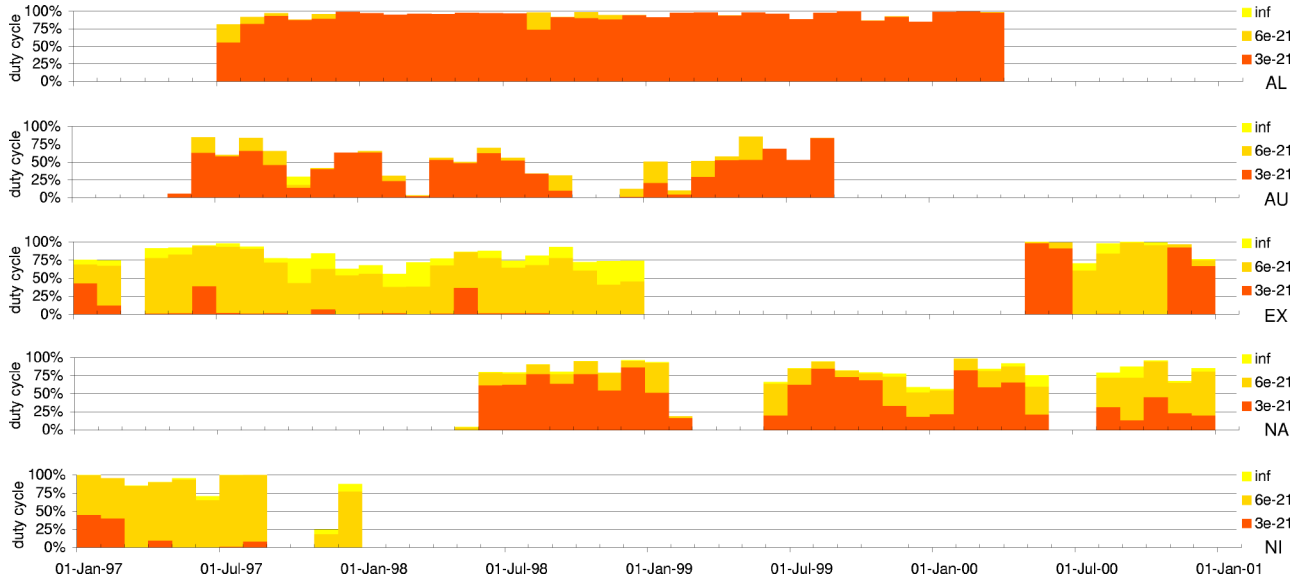


FIG. 2. Overview of the observation periods in 1997–2000 for each detector, as fractions of time in monthly bins. Three different ranges of sensitivities are considered: exchange threshold lower than $3 \times 10^{-21} \text{ Hz}^{-1}$ (darker shade), included in $3\text{--}6 \times 10^{-21} \text{ Hz}^{-1}$ (middle shade), and above $6 \times 10^{-21} \text{ Hz}^{-1}$ (light shade).

thus the rate of false alarms of the observatory.

The search for time coincidences among events of different detectors is performed by setting variable time windows computed from the ETA uncertainties to ensure a certain probability of false dismissal (see Sec. III B). A rough estimate of the contribution of each individual detector to the final rate of accidental coincidences of the observatory can be found by considering the product of its average ETA standard deviation σ_t and its average event rate $\bar{\lambda}$.⁵ The IGEC recommendation is that the threshold be kept high enough so that

$$\frac{\bar{\sigma}_t \times \bar{\lambda}}{T_{\text{obs}}} = \frac{\sum_{i=1}^n \sigma_{t_i}}{T_{\text{obs}}} < 0.1\%, \quad (2)$$

where σ_{t_i} is the standard deviation of the arrival time for the i th event, n is the total number of events, and T_{obs} is the total observation time. This recommendation is an improvement of the one followed in the previous data exchange, i.e., to limit the rate to 100 events per day [19], in order to cope with the widening of the effective bandwidth of the detectors.

The ETA standard deviation has been estimated by means of a Monte Carlo simulation for the AURIGA, EXPLORER, and NAUTILUS detectors [18,20] or by measuring the response of the detector to repeated impulsive excitations for the ALLEGRO detector [1]. The uncertainty in the ETA depends both on the noise level and on the timing accuracy of the filtered data. Therefore, the behavior of σ_t is significantly different for the different detectors, though it decreases in all

of them as the SNR increases. It was also found to vary with time in AURIGA, EXPLORER, and NAUTILUS, following the variations of the effective bandwidth of the detector [20,21]. Typical values of $\bar{\sigma}_t$ have been fractions of a second.

Whenever environmental monitors have been operating, the events have been checked against periods of ambient disturbances prior to their exchange. If an event from the filtered data occurs in coincidence with an excitation observed by these monitors, it is vetoed and not considered a candidate GW event. For AURIGA, no veto based on an environmental monitor has been implemented, yet the event has to pass a χ^2 test to check its consistency with an impulsive mechanical excitation of the bar [16]. This test has been found to provide a good reduction of false alarms at high SNR. Despite all such efforts to remove local excitations in the detectors, most of the events above threshold cannot be ruled out as candidate GW events [22]. Partial information

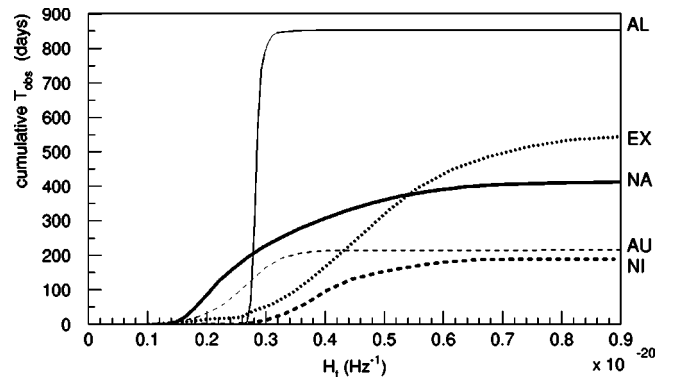


FIG. 3. Observation time of the IGEC detectors as a function of a threshold H_t on GW amplitude in 1997–2000. The ordinate is the integrated time during which the detector exchange threshold has been lower than H_t .

⁵See, for instance, Eq. (1) of Ref. [12], valid in the simple case of equal time uncertainties and uncorrelated noise performances. A more general discussion can be found in Ref. [21].

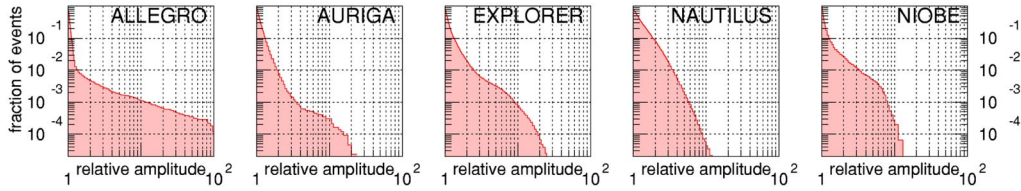


FIG. 4. Cumulative distribution function of the amplitude of the exchanged events: the ordinate is the fraction of events whose amplitude is greater than the value in abscissa. The amplitude is normalized to the corresponding exchange threshold of the detector.

about vetoed events is tracked in the exchanged event lists for diagnostic purposes.⁶

C. Data overview

The duty cycle of the network has been previously reported in detail [13,19]. A graphical representation of the on-off times of the individual detectors between 1997 and 2000 is shown in Fig. 2. During this 4 year period, there were 1319 days when at least 1 detector was operating, 707 days with at least 2 detectors in simultaneous operation, 173 days with at least 3 detectors and 26 days with at least 4 detectors. This time coverage is a consequence of the non-optimal overlap among the operating times of the single detectors and of their duty cycles, which were included within the 0.9 achieved by ALLEGRO and the 0.3 of AURIGA.

The cumulative observation time of each detector versus GW amplitude is shown in Fig. 3. The exchange thresholds of the detectors fluctuated significantly in time for all detectors but ALLEGRO, following the nonstationary behavior of the noise.

The typical range of the exchanged thresholds was $2-6 \times 10^{-21} \text{ Hz}^{-1}$. Neglecting the directional sensitivity of the detector, this range corresponds to a 1-ms burst generated by $(0.02-0.2)M_{\odot}$ solar masses converted in GWs with isotropic emission at a distance of 10 kpc. With respect to the first IGEC data exchange [19], EXPLORER and NAUTILUS take the opportunity of the relaxed recommendation on the average rate of exchanged events [Eq. (2)] and lower the exchange threshold (from $\text{SNR} \approx 5$ to about 4.5). The data of the other detectors keep the previous exchange thresholds ($\text{SNR} \approx 3$ for ALLEGRO and NIOBE, $\text{SNR} \approx 5$ for AURIGA). The mean rate of events exchanged by EXPLORER and NAUTILUS is about 5 times greater than in the previous exchange, while for the other detectors it remains at the same level.

The amplitude distributions of the exchanged events are shown in Fig. 4. At least two distinct regimes are observed in all detectors, though showing a large variability among them: a steep roll-off close to the threshold and an additional tail dominating at SNR greater than ~ 10 . The exchanged events are mostly generated by non-Gaussian noise

sources, which are not currently modeled.

The average number of events observed in each hour (universal time) is shown for the five detectors in Fig. 5. All detectors show an increase in the number of events observed at certain hours of the day. For AURIGA, EXPLORER, and NAUTILUS, higher event rates are observed between 5 and 18 h local time, while for NIOBE between 7 and 16 h local time. Such behavior is consistent with a correlation with human activity. The event rate for ALLEGRO is almost constant and shows a small increase between 18 and 23 h local time. Note that since AURIGA, EXPLORER, and NAUTILUS are in the same time zone, the rise and fall of event rates is almost synchronized.

The average rates of the events exchanged by each detector are shown in Fig. 6 as a function of an absolute *search threshold* on the GW amplitude. The search threshold is applied to each event list before performing the coincidence search described in Sec. III B. For a given search threshold value H_t , the rate is computed dividing the number of events exceeding H_t by the observation time during which the exchange threshold of the detector has been lower than H_t . This procedure is consistent with the data selection we applied in the multidetector analysis, as described in Sec. III A. In general, the event rates decrease as the search threshold increases because the number of selected events decreases and the selected observation time increases. However, this can happen in a nonmonotonic way due to the nonstationary behavior of the noise performances of the detectors. In fact,

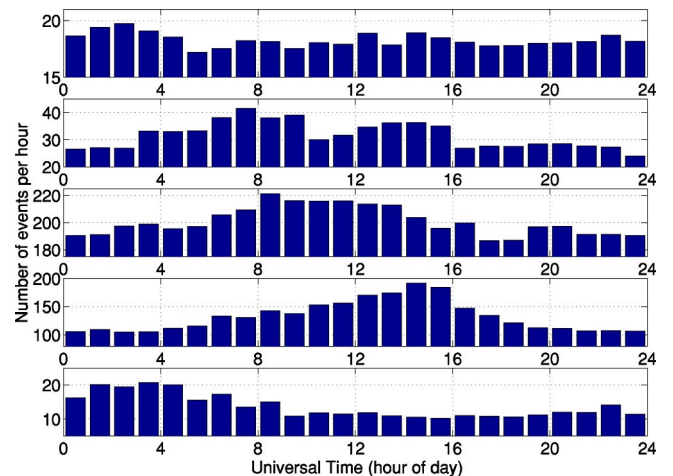


FIG. 5. Average rate of exchanged events per each UTC hour of the day. From top to bottom: ALLEGRO, AURIGA, EXPLORER, NAUTILUS, and NIOBE.

⁶For instance, the vetoed events have an associated dead time which have to be taken into account when computing the false dismissal of the observatory. In practice this amounts to removing a negligible fraction of the observation time.

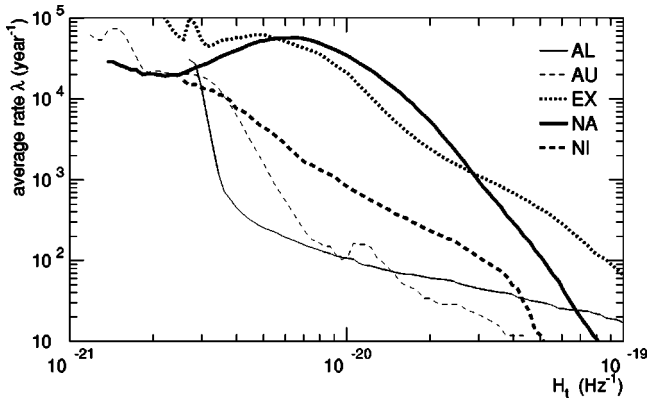


FIG. 6. Average rate of the events exchanged by the detectors as a function of a threshold H_t on GW amplitude, as described in the text. The minimum threshold plotted for each detector corresponds to 10 days of observation time.

as the search threshold increases, the selected observation time can extend to additional periods of operation characterized by worse sensitivity. These periods contribute with a much higher instantaneous rate of events, given that most events appear very close to the exchange threshold (see Fig. 4). Therefore, the mean event rate may increase at some higher search threshold.

The mean timing uncertainty $\overline{\sigma_t}$ of the exchanged events is shown in Fig. 7 for each detector as a function of the search threshold. The value of $\overline{\sigma_t}$ is dominated by the selected events which are closest to the exchange threshold of the detector. As the threshold increases, the mean timing uncertainty decreases down to the limit given by the timing calibration or resolution of the detectors, which is in the range 1–80 ms. Similarly to Fig. 6, $\overline{\sigma_t}$ is a nonmonotonic function of the search threshold due to noise being nonstationary. For instance, the peak shown by AURIGA data around 10^{-20} Hz^{-1} is due to a 1-week period of operation of the detector with reduced sensitivity and reduced effective bandwidth. For the NIOBE data a conservative estimate of

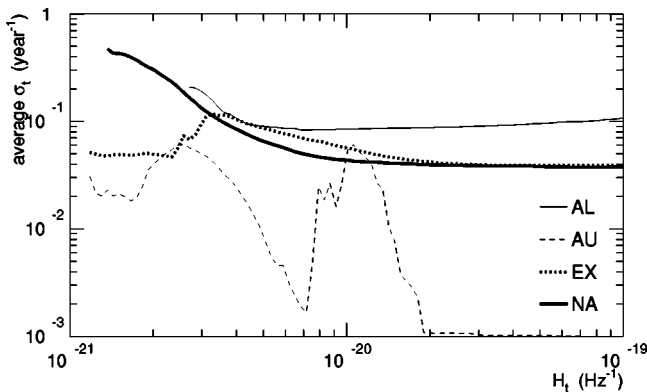


FIG. 7. Average standard deviation of the ETA of exchanged events, $\overline{\sigma_t}$, as a function of a threshold H_t on GW amplitude, as described in the text. The minimum threshold plotted for each detector corresponds to 10 days of observation time. For NIOBE only a 1-s upper limit for the time standard deviation is available.

$\overline{\sigma_t}$ was provided, independent from the event amplitude.

Figures 6 and 7 allow the reader to compare the contributions of each detector to the false alarm rate of the observatory as a function of the selected threshold H_t on GW amplitude. In this respect, the quality of the detector is given by the product of the mean event rate and the mean uncertainty of the ETA, as already discussed in connection with Eq. (2). The cleanest detectors have been ALLEGRO and AURIGA in the investigated range of GW amplitudes. To be precise, the actual false alarm rate of the observatory is not directly related to the mean event rates. Rather it is time by time proportional to the product of the instantaneous event rates of the participating detectors [21]. Moreover, the dependence of the actual false alarm rate on the uncertainties of the ETA is also not simple: since the larger timing uncertainties dominate the time window used for the coincidence search (see Sec. III B), the role of the detectors showing the worst timing performance is enhanced.

D. Event time series statistics

In a time coincidence search, the statistics of the estimated time of arrival of the events plays a fundamental role. In case the event times are random, a Poisson point process would fit the data. Actually, the data do not reproduce a homogeneous (i.e., stationary) point process, due to the changing performance of the detector and to the statistics of outliers. For our purposes, it is enough to check time scales below ~ 1 h, because they are critical for the method implemented to estimate the noise background (see Sec. III D).

In order to investigate the ETA statistics of IGEC exchanged data we calculate their correlation histograms (or *correlograms*) as shown in Fig. 8. Correlograms are histograms of the time lags between ETAs. For a Poisson process one expects the histogram to be flat—i.e., without preferred time delays between events (see Appendix A for details). It turns out that the ETAs show relevant autocorrelation at small time scales, down to a few seconds. A clustering of the event time series for all the five IGEC detectors is evident. The clustering disappears as soon as one looks to the cross-correlation properties. This is very relevant for the next phase (i.e., coincidence search), because if this were not the case, the output of the empirical method we use to estimate the background would be biased (see Sec. III D).

III. MULTIPLE DETECTOR ANALYSIS

In this section we present the methods implemented by the IGEC to analyze the exchanged data. The analysis is based on a time coincidence search among GW candidates, or events, of different detectors (see Sec. III B). The time coincidence window is varied to get the desired maximum probability of false dismissal. We discuss also a test of the compatibility of the signal amplitude, as estimated by the different detectors (see Sec. III C). Prior to the coincidence search, we apply a data selection procedure which limits the search to burst GWs exceeding a specified search threshold (see Sec. III A). A directional search strategy is implemented as well. The IGEC analysis is then performed as a function

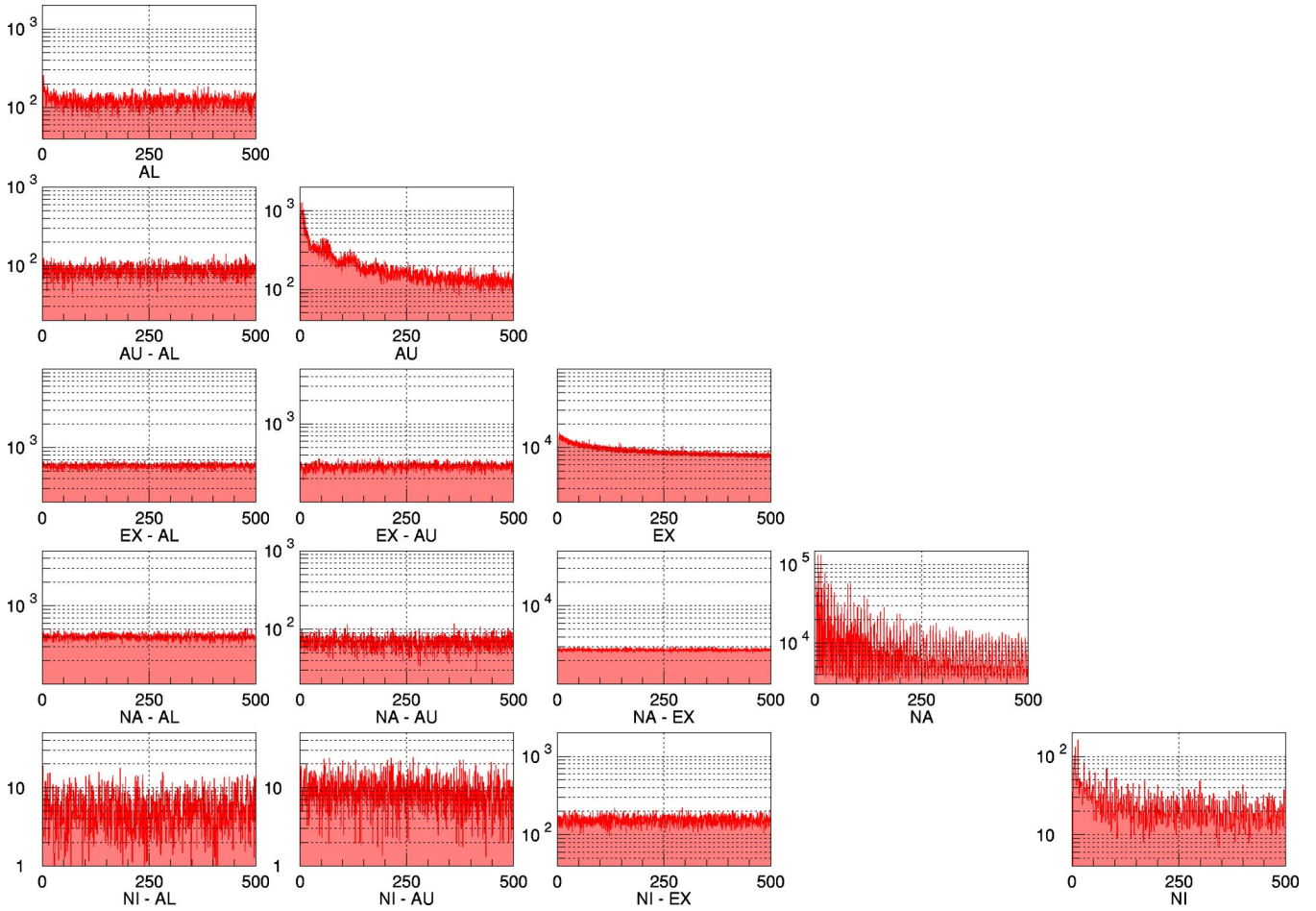


FIG. 8. Correlogram matrix for the estimated time of arrival of all exchanged events in the years 1997–2000; all plots are histograms of the time lags between events in units of counts/s (*ordinate*) vs seconds (*abscissa*). All five autocorrelation histograms of the single detectors (*diagonal plots*) show correlation at short time scales, and in three cases these structures dominate by far over the uniform distribution expected in case of a Poisson process. Despite this, the cross correlograms (*off-diagonal plots*) show no sign of residual correlation. The NA-NI cross correlogram is empty because these two detectors had no overlap in their operative time.

of the search threshold value and of the GW direction. The main advantages of this procedure are a reduction in the false alarm rate and the control of the maximum probability of false dismissal of any burst GW exceeding the search threshold. The accidental coincidence background has been estimated by applying the same analysis procedures on many data sets obtained by shifting the time of the real data (see Sec. III D). The first relevant result of this analysis is that the number of estimated accidental coincidences turns out to be a Poisson random variable. Finally, in Sec. III E we describe the statistical method used to set the confidence intervals on the number of GW bursts detected by the observatory. This method is *unified* and ensures the desired coverage of the resulting confidence intervals.

A. Data selection

Before searching time coincidences, we apply a data selection procedure which limits the search to burst GWs exceeding a specified amplitude.

The first step is to specify an absolute threshold H_t , or *search threshold*, for the GW amplitude estimates. This threshold is common to all detectors and sets the lower bound on the amplitude of the target GW population. The following multiple detector analysis is then repeated systematically for different threshold values.

The second step is to exclude from the observation time of each detector all time periods where the exchange threshold is *above* the chosen search threshold. The motivation is to limit the false dismissal probability of any burst GW of amplitude greater than the selected threshold. With this selection, the detection efficiency for burst GWs exceeding H_t is at least 0.5 in any detector.

The third step is to exclude candidate events that are *below* the search threshold. This gives a significant reduction of the false alarms, while preserving the same minimum detection efficiency of the previous step. In fact, the exclusion of the lower amplitude events cuts down both the rates and the time uncertainties of the events of each detector (see Figs. 6 and 7).

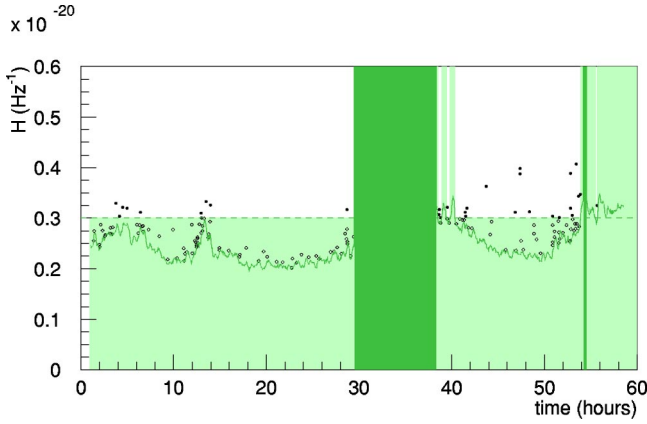


FIG. 9. An example of the selection on AURIGA data for a search not optimized for a specific GW direction. The continuous gray line shows the amplitude of the exchange threshold; the dots represent the exchanged events vs time. In the dark gray period no data were exchanged. The light gray shaded area shows the amplitude-time regions excluded by the data selection at a search threshold $H_t = 3 \times 10^{-21} \text{ Hz}^{-1}$. The observation times with exchange threshold $> 3 \times 10^{-21} \text{ Hz}^{-1}$ are now excluded as well as the events with amplitude $< 3 \times 10^{-21} \text{ Hz}^{-1}$.

This procedure differs from what have been previously done in the field.⁷ The data selection is illustrated in Fig. 9 with a sample of AURIGA data. In general, a higher search threshold H_t allows new portions of the observation time to be considered, thus increasing the effective observation time. Moreover, the rate of the selected events will strongly depend on the value of the detector exchange threshold with respect to H_t . In particular, higher rates of events are favored whenever the exchange threshold approaches and crosses the search threshold.

The described data selection is suitable for a blind search over the sky, irrespective of the source location. In fact, a burst GW is seen at each detector with the same amplitude, given that the antenna patterns are almost coherent.

It is also possible to implement a directional search strategy to optimize the search for a specific GW direction. This has been accomplished by modulating the exchanged data with the directional sensitivity of the detectors. Specifically, all exchanged amplitudes (event amplitudes, exchange thresholds, etc.) are divided by the time-dependent angular sensitivity factor for the specific direction in the sky (see Fig. 1). In this way, all amplitudes are given in terms of a burst GW propagating from the selected direction. Figure 10 shows the search for burst GWs from the galactic center direction on the same data set of Fig. 9. Then, the rest of the

⁷In some previous analyses [8,9], a systematic study has been made as a function of the amplitude of the events but not of the sensitivity of the detectors so as to ensure a minimum detection efficiency. In the others [10,11,26], the observation time has been selected according to some fixed threshold on the detector noise and no common thresholding on the amplitude of events have been performed.

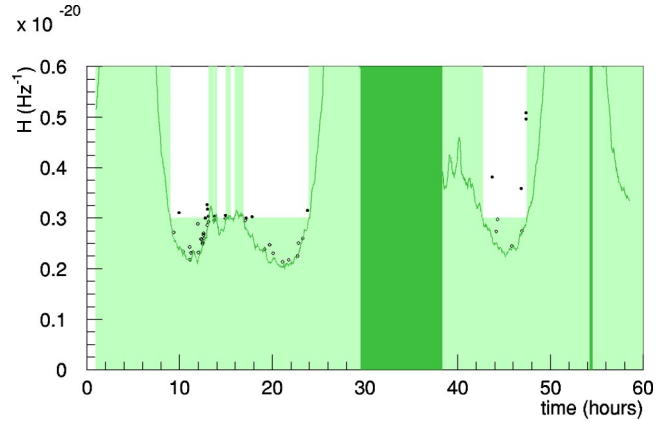


FIG. 10. The same data of Fig. 9 but now specialized to a search for gravitational wave bursts from the galactic center. The exchange threshold (gray line) and events (dots) have been divided by the amplitude directional sensitivity of the detector to the galactic center. The resulting amplitudes are in terms of a burst GW from the galactic center. The light gray shaded area shows the amplitude-time regions excluded by the data selection at a search threshold $H_t = 3 \times 10^{-21} \text{ Hz}^{-1}$.

selection procedure above is applied. The effective observation time is reduced with respect to that obtained for a blind search over the sky at the same threshold H_t , because the periods when the detector is not favorably aligned with the source are removed. Additionally, the set of selected events is generally different.

As a result, the background noise is reduced while the detection efficiency for the selected direction is preserved. It is worth noticing that the angular selectivity of any directional search is quite poor, due to the broadness of the directional sensitivities of the detectors. For instance, when the detector is optimally oriented with respect to the chosen direction, any source within $\pm 20^\circ$ from it is seen with at most 11% attenuation.

The modulation by the directional sensitivity correlates the amplitudes of events and exchange thresholds among different detectors in a much more significant way than any other observed daily effect. This modulation produces new cuts to the observation time and related clusters of events which are almost synchronized in different detectors. As a consequence, the probability of coincidences is enhanced at the edges of the time spans of common observation. The effects of this when estimating the rate of accidental coincidences is discussed in Sec. III D.

We note that the false dismissal contributed by this data selection is at most 50% per each detector for burst GWs of amplitude exceeding the chosen search threshold H_t . The overall false dismissal of this multiple detector analysis will be further increased by the next two steps, namely, the time coincidence search and the amplitude consistency check (see the following sections). However, the overall false dismissal for a burst GW above H_t is under control at least in a conservative sense. The optimal range of H_t values that would enhance the chances of GW detection will depend also on the (unknown) amplitude distribution and rate of the burst GWs.

B. Time coincidence search

Two events from different detectors are defined to be in coincidence if their estimated times of arrival t_i and t_j are compatible within their variances $\sigma_{t_i}^2$ and $\sigma_{t_j}^2$:

$$|t_i - t_j| \leq \Delta t_{ij} \equiv (k \sqrt{\sigma_{t_i}^2 + \sigma_{t_j}^2} + \Delta t_{\max}), \quad (3)$$

where Δt_{ij} is the coincidence window and Δt_{\max} is the maximum expected light travel time between the detectors. Δt_{ij} is computed according to the desired probability of false dismissal by setting k through a Bienaymè-Tchebyscheff inequality.

Specifically, the probability to miss a coincidence because of the uncertainties in the ETA is

$$FD \equiv P\{|t_i - t_j| \geq \Delta t_{ij}\},$$

which in turn is upper bounded by

$$FD \leq P\{|t_i - t_j| \geq k \sqrt{\sigma_{t_i}^2 + \sigma_{t_j}^2}\} \leq \frac{1}{k^2} \equiv P_T, \quad (4)$$

where P_T is the maximum false dismissal probability chosen for the coincidence search (see Appendix B). The resulting coincidence window changes for each couple of events according to their ETA variances.

This procedure ensures that the required maximum false dismissal probability is met regardless of the distribution of the estimated arrival time uncertainties. In fact, it is not possible in general to approximate the ETA statistics as Gaussian, due to either the intrinsic narrow bandwidth of the detectors or their limited time resolution. For instance, in the AURIGA data the time accuracy has been 1 ms and the time uncertainty distribution is multimodal [23] at the SNR of interest. The ETA standard deviation is then dependent on the SNR of the event. We note that $\sigma_t \gg \Delta t_{\max}$ is the standard condition in these IGEC data. For comparison, the previous IGEC preliminary analysis [12] has been performed with a fixed value for the coincidence time window and therefore only a vague indication of the false dismissal was possible.

The implemented coincidence search allows one event to be in coincidence with more than one event in the other detector. A coincidence in more than two detectors has to satisfy Eq. (3) for all combinations of detector pairs, and the resulting conservative false dismissal has to take into account the number of such required conditions. The same time coincidence search algorithm has been applied both to actually search for burst GWs and to estimate the corresponding number of accidentals (see Sec. III D).

The choice of the conservative false dismissal P_T due to the coincidence search can be optimized (see Appendix B). It turns out that P_T should be set between 30% and 5% to achieve a satisfactory balance between false alarm and false dismissal probabilities in a twofold coincidence search.

C. Amplitude consistency check

The estimated amplitude of a burst GW is affected by the systematic and statistical uncertainties of the detector. Hence,

once the members of a set of events are found to be in coincidence, one can test if the differences of their estimated amplitudes are consistent with zero within a chosen confidence level. The goal is to lower the false alarms by removing the accidental coincidences whose amplitudes are not consistent. The test we implemented is similar to the condition described above to define a time coincidence.⁸ It takes into account both the variance $\sigma_{A_i}^2$ and the fourth central moment $\mu_{A_i}^{(4)}$ of the estimated amplitude of the events A_i , which are included in the current IGEC exchange protocol.

Two events from different detectors have consistent amplitudes if

$$|A_i - A_j| \leq \Delta A_{ij} + \Delta A_i + \Delta A_j, \quad (5)$$

where

$$\Delta A_{ij} \equiv \min \left\{ \sqrt{\frac{\sigma_{A_i}^2 + \sigma_{A_j}^2}{P_A}}, \sqrt[4]{\frac{\mu_{A_i}^{(4)} + \mu_{A_j}^{(4)} + 6\sigma_{A_i}^2\sigma_{A_j}^2}{P_A}} \right\}$$

and ΔA_i are the systematic amplitude calibration errors of the detectors. P_A is the required conservative false dismissal of the test for a coincidence which corresponds to a burst GW. The two alternative terms in curly brackets come from the Bienaymè inequality of second and fourth order, respectively, applied to the random variable $A_i - A_j$. The more stringent of them is chosen time by time (see Appendix B).

The general Bienaymè inequality is used because the amplitude noise distributions of the detectors were not Gaussian or modeled for a significant fraction of the observation time. This test is conservative and provides a less stringent removal of false alarms at low SNR amplitudes with respect to tests based on some modeled statistics. Instead, at high SNR amplitudes the systematic calibration errors, 10% for all detectors, dominate over ΔA_{ij} .

The efficiency of the false alarm rejection of this amplitude consistency test was found to be strongly dependent on the search threshold. The false alarms were significantly reduced only at high thresholds, $H_i \geq 1 \times 10^{-20} \text{ Hz}^{-1}$. This is due to two concurrent facts. First of all, the implemented data selection forces most of the events to have similar amplitudes, since they are constrained from below by the imposed search threshold and from above by the steep slope of the amplitude distribution (Fig. 4). Therefore, the data preprocessing itself provides an implicit rejection of most of the events in coincidence which show nonconsistent amplitudes. Second, the efficiency of the test is greater at high SNR amplitudes, because there the amplitude differences of accidental events can be larger in terms of standard deviations.

As a result, the test turned out to be convenient only at high search thresholds and with values of conservative false dismissal $P_A < 30\%$. On the contrary, at low thresholds the implementation of the test is disadvantageous because the

⁸Different amplitude consistency tests has been applied to coincidence searches with other data sets. The procedures and the results are reported in Refs. [11,26,31].

increase in the false dismissal is not balanced by a sufficient false alarm reduction. For the results described in this paper, the application of this amplitude consistency test did not add new significant information.

D. Background estimation

In order to assess the statistical significance of the number of detected coincidences, a reliable estimate of the background—i.e., the number of coincidences that have been found by chance—is needed. The ideal approach would be to obtain new independent data sets from a population with the same statistics, but with all GW sources switched off, to repeat the search procedure and then to compare the statistics of the found coincidences with those obtained from the original sample.

If the ergodic hypothesis applies to our data, a good method to create an independent data sample is to perform a relative translation of the time coordinate of the data exchanged by different detectors. This operation preserves the statistics of the single event list (average number of events, instantaneous rate fluctuations, autocorrelation of event times, etc.). The coincidence counts found on time shifted data sets are independent as long as the applied time delays are longer than the maximum time window used in the coincidence search. It is reasonable to assume that the GW events are a negligible fraction of the *total* number of events at each detector and therefore the GW events will not affect the coincidences within the shifted data sets. This empirical method has been widely used in the field (see, for instance, [8–12]). We remark that this framework allows us to only estimate the level of the coincidence background, but not to distinguish between coincidences due to GWs and those due to other common sources.

There are a number of technical subtleties to address in order to give a complete description of the way this method has been practically implemented in this analysis. One issue regards the common observation time of each time shifted configuration, i.e., the collective length of the time spans after the data selection phase. In fact, in case of significant changes of the shifted observation time one should consider the *rates* rather than the counts of accidental coincidences, but then the statistics of this random variable is no longer Poissonian.

Another crucial issue is to check the statistics of the background, especially in IGEC data, since the statistics of the event time series of each detector shows evidence for autocorrelation at small time scales (see Fig. 8). We require that the statistics of the coincidence background estimates be Poissonian and stationary for any applied time shift, as is expected if the coincidence time series can be modeled by a Poisson point process. In fact, this is the model we use in Sec. III E to estimate the statistical significance of the found coincidences with respect to the background. Note that the instantaneous coincidence rate may be also time varying (i.e., nonhomogeneous), and still the coincidence counts in a fixed time span of a shifted configuration would be a sample of a Poisson random variable. Independence (i.e., randomness) of successive coincidence times is the key to guarantee

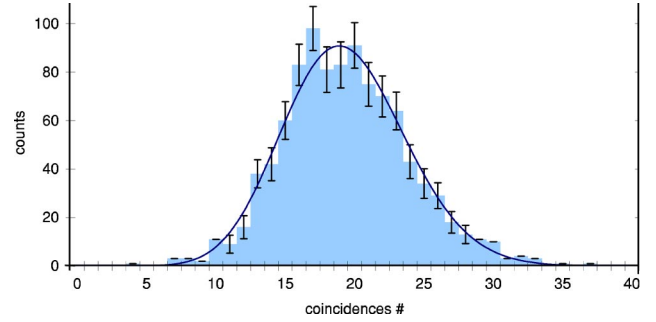


FIG. 11. Sample of the histogram of the background coincidences obtained by the time shift method with a superimposed Poisson fit. The plot shows the shifted coincidences between EXPLORER and NAUTILUS searched with $P_T=5\%$, $P_A=0$, and search threshold of $5.62 \times 10^{-2} \text{ Hz}^{-1}$ without optimizing for a GW direction. The one tail χ^2 probability of the sample is 0.7. The χ^2 test is performed only on the histogram bins with at least 10 counts. The maximum time shift reached ± 5000 s in 10-s steps.

this result. This requirement is met when the event lists are not cross correlated within time scales up to the maximum applied time shift.

When performing a search optimized to a specific direction (Sec. III A), we pointed out the additional problem related to the appearance of clusters of events at times correlated in different detectors. In this case the key for a successful estimation of the background has been to time shift the data *before* applying the amplitude modulation.

In this analysis, the number of tested time-shifted configurations for a pair of detectors is $N_s \sim 1000$. This number is limited by two requirements. The first is to keep the shift step larger than the longer time window used for coincidence search. On the other hand, the maximum delay has to be small enough to keep stationary the random variable number of accidental coincidences. The maximum time shift has been limited to $\sim 5 \times 10^3$ s and the shift steps has been between 5 and 15 s.

The easiest way to check the Poisson statistics and the independence of the background samples is to create an histogram of the number of coincidences found at each time shift and fit it to a Poisson density function. Figure 11 shows the agreement of the background statistics to the model for a sample configuration. To test the goodness of the Poisson fits we applied chi-square tests whenever the histograms of the background counts were sufficiently populated. The probability of getting a chi square greater than the observed value has to be a sample of a uniform density between 0 and 1 if the performed fit is good. This has been actually confirmed, as shown by the histogram of the resulting one-tail chi-square probabilities shown in Fig. 12; therefore, we can conclude that no deviations of the background estimates from the expected Poisson statistics are observed.

We remark that this is a quite relevant result, since in our case the single event lists showed evident autocorrelation at short time scales (see Fig. 8) and since the GW search from a specific direction brings in a significant correlation of the selected event rates in different detectors, as described in Sec. III A. As a consequence, we have been able to use all

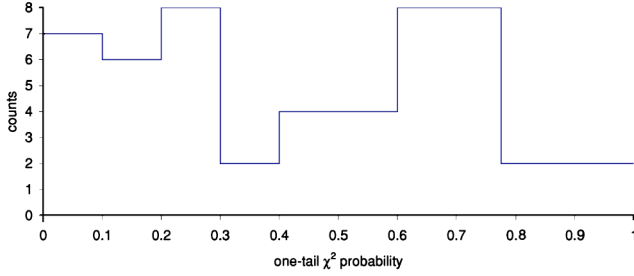


FIG. 12. Histogram of the significance level of the goodness-of-fit test for the Poisson model of the background estimates (one tail χ^2 probabilities). The χ^2 test has been performed on all the configurations of the observatory which ensured at least one degree of freedom (see Fig. 11). The plotted data include configurations of different detectors with different search threshold values and same conservative false dismissal of the coincidence search ($P_T = 5\%$, $P_A = 0$), without optimizing for a GW direction. The maximum time shift reached 5000 s in 10-s steps. The histogram is well described by a uniform distribution, so we can conclude that the χ^2 tests give results consistent with a general agreement of the background statistics to the Poisson model.

the available data to set confidence intervals on the detected GW with the procedure described in the following section.

E. Setting confidence intervals on detected GWs

The found number of coincidences and the expected background are compared under the hypothesis of a superimposed homogeneous Poisson rate of detected GW signals. The results are then expressed as confidence intervals containing the true rate of detected GWs with a given probability, i.e., assuring a given *coverage*. The procedure we adopt to set confidence intervals follows the track of previously reported *unified* methods [24,25]. The results will be interpreted either as upper limits or as evidence for detection in case the confidence intervals include or not the null result.

We assume a Poisson model for the coincidence background, whose expected number \bar{N}_b is estimated as described in the previous subsection. Having observed a number of actual coincidences N_c , the likelihood function of the average number of detected GWs, N_Λ , is

$$\ell(N_\Lambda; N_c, \bar{N}_b) \equiv \begin{cases} P_{N_c}(\bar{N}_b + N_\Lambda) & \text{if } N_\Lambda \geq 0, \\ 0 & \text{if } N_\Lambda < 0, \end{cases} \quad (6)$$

where

$$P_{N_c}(\bar{N}_b + N_\Lambda) \equiv \frac{1}{N_c!} (\bar{N}_b + N_\Lambda)^{N_c} e^{-(\bar{N}_b + N_\Lambda)}. \quad (7)$$

Then the confidence interval is defined by integrating the likelihood over the smaller domain $[N_{\text{inf}} - N_{\text{sup}}]$ which ensures that the integral amounts to a specified value I :

$$I = \left[\int_0^\infty \ell(N) dN \right]^{-1} \int_{N_{\text{inf}}}^{N_{\text{sup}}} \ell(N) dN. \quad (8)$$

The intervals defined as such have nice properties [25]. First, they are naturally bound to the physical domain. Moreover, they include the most likely estimate of the number of detected GWs, which is zero when the expected background exceeds the found number of coincidences. Such most likely confidence intervals are also the *most credible* in the Bayesian framework assuming a uniform prior for $N_\Lambda \geq 0$. However, when the value for the likelihood integral I is properly chosen, the resulting interval has also a well-defined minimum frequentist coverage. From numerical computations it turns out that $I = 0.94$ and $I = 0.97$ guarantee the coverage to be at least 0.90 and 0.95 respectively. By taking into account the effective observation time, the confidence intervals can be expressed in terms of the Poisson rate of detected GWs.

The overcoverage ensured by this unified method is quite significant for true GW rates much less than the background rate. In particular, in case the true value is exactly zero (null hypothesis) the complement of the coverage to unity can be interpreted as the false detection probability, and it is lower than $\sim 4.5\%$ and $\sim 2.3\%$ when the conservative coverage is respectively 0.90 and 0.95.

IV. RESULTS

The IGEC observations have been analyzed both by performing a blind search over the sky (without selecting a specific GW direction) and by optimizing the search for burst GWs from the galactic center direction. In the first case the results refer to the amplitude component of the burst GWs along the detector axes. In the second case the results are given in terms of the amplitude of a burst GW from the galactic center. In both cases, only the polarization component along the bar axis is considered.

We define the operating time of a particular *configuration* of detectors to be the subset of the network operation periods when only the detectors of this configuration are simultaneously operative. The main advantage of this procedure is that the results from different configurations are then automatically *independent*, since they refer to disjoint observation times. We remark that the operating times of the configurations depend on the search threshold (see Sec. III A). Within IGEC, 18 different configurations of detectors have been operating during 1997–2000: 9 pairs, 7 triples and 2 fourfold configurations. The multi-detector data analysis has been performed separately for each configuration as a function of the search threshold H_t in the range $2 - 50 \times 10^{-21} \text{ Hz}^{-1}$.

In order to synthesize the overall result of the observatory at each threshold value, we sum the observation times, coincidence counts, and backgrounds over all the configurations at the same H_t . A confidence interval of the whole network is then recomputed accordingly for each H_t .

We report a synthesis of the results (number of coincidences, background, observation time, confidence interval on

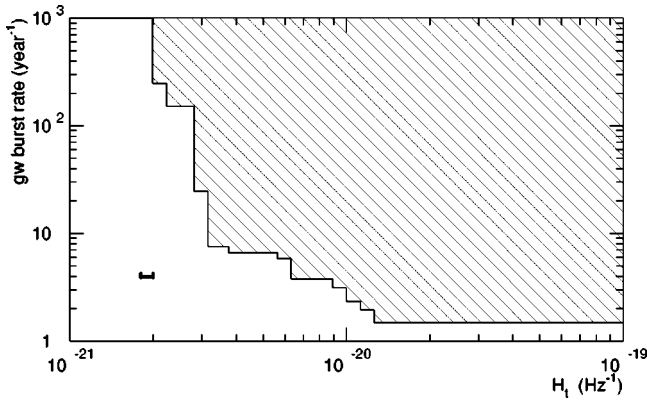


FIG. 13. Upper limit for the rate of the burst GWs detected by the observatory as a function of the amplitude search threshold H_t . No directional search has been applied (i.e., blind search over the sky). The Fourier amplitude in abscissa refers to the component of a burst GW along the axes of the detectors. The dashed region above the solid line is excluded with at least 95% probability. The uncertainties on the estimated background affect negligibly the plotted curve. The time window for the coincidence search has been selected to limit the related false dismissal probability to at most 5% and no test on the amplitude consistency between events has been applied. The maximum amplitude systematic error related to the calibrations of the detectors is shown as the error bar parallel to the abscissa.

detected GWs) for each configuration of detectors and investigated threshold value in Appendix C. The results depend also on the choice of the parameters of the analysis, namely, the false dismissal on the time coincidence search, the false dismissal on amplitude consistency of events in coincidence, the selection of a direction in the sky, and the required conservative probability, or *coverage*, of the confidence intervals.

The results obtained at each threshold value are cumulative: i.e., they apply to detected burst GWs whose amplitudes are $\geq H_t$. This is a consequence of the data selection described in Sec. III A. In particular, an upper limit set at some threshold H_t is valid with the same conservative coverage for any higher threshold.

A. No statistical evidence for detected GWs

The overall results over the entire time span 1997–2000 are well in agreement with the estimated background. In fact, the resulting confidence intervals on the number of detected GW signals include the null result in almost all the many trials performed (see Appendix C). Only a few twofold configurations give GW detections for some specific values of the parameters of the analysis. We will show, however, that the relative frequency of these cases is well accounted for by the probability of false alarm, i.e., of getting by chance a detection in case no GW were present in the data.

The probability that a confidence interval may fail to include the null result in case no GWs are present in the data

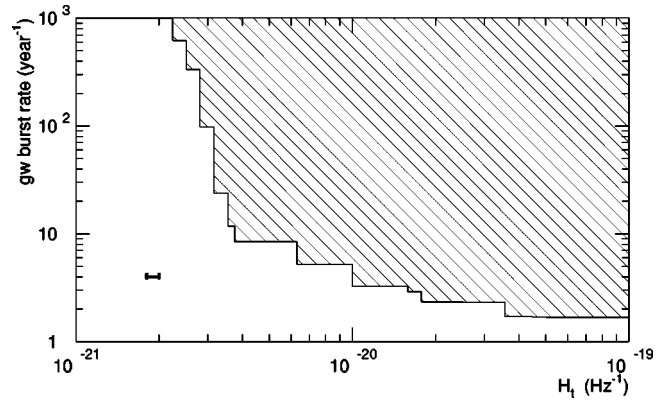


FIG. 14. Same as Fig. 13, but specialized for the rate of burst GWs from the galactic center direction. The Fourier amplitude in abscissa refers to the amplitude of a burst GW from the galactic center direction with optimal polarization with respect to the detectors.

has been numerically computed by simulating the procedure to set confidence intervals (see Sec. III E). As a result of the overcoverage of these confidence intervals, this probability is always smaller than the maximum false dismissal associated to the interval, i.e., $1 - \text{coverage}$, especially at low background levels. Specifically, when the accidental coincidences are $\bar{N}_b \geq 1$, the expected number of false alarms oscillates around $\sim 3\%$ and $\sim 1.5\%$, respectively, for maximum false dismissal values of 10% and 5%. This means that false alarms of the order of one every 30 (r. 70) independent trials are the rule in case of $\bar{N}_b \geq 1$. Instead, in the limit of low background, i.e., $\bar{N}_b < 0.01$, the false alarm probability turns out to be \bar{N}_b regardless of the required coverage. Therefore no false alarms are expected for the configurations showing low enough background levels. These predictions on false alarms obtained by numerical simulations have also been confirmed by an independent empirical method (see Appendix C).

No statistical evidence for detected GWs has been found. In fact, on the one hand, the null result is always included in the confidence intervals corresponding to low background levels, such as those related to threefold and fourfold configurations of detectors. On the other side, the total number of detections is consistent with the total number of expected false alarms. For the many trials reported in Appendix C, the expected {found} total numbers of false alarms for the galactic center search are 3.5 {2} and 1.7 {0} for 0.9 and 0.95 coverages, respectively. For the blind search over the sky these numbers are 2.5 {4} and 1.4 {2}.

With at least three IGEC detectors in simultaneous operation the false alarms are extremely rare even at search thresholds H_t close to the exchange thresholds of the single detectors. So even after many years of observation time, such configurations would allow one to easily identify any detected GW. Instead, in the case of a twofold coincidence search, the false alarms populate the achieved observation time up to high search thresholds, $H_t \leq 10^{-20} \text{ Hz}^{-1}$.

B. Upper limit on the rate of detected GWs

The resulting IGEC observations can be synthesized by an upper limit on the rate of detected burst GWs, modeled as a Poisson point process with constant rate. This upper limit as a function of the signal search threshold is given in Figs. 13 and 14 for a search not optimized for any specific direction and optimized for the galactic center direction, respectively. These upper limits are based on the confidence intervals of the network, computed from the sums of the data (observation times, coincidence counts, and background) of all configurations per each threshold value. The plotted upper bounds have a probability of at least 95% to be greater than the actual GW rate value, so that the dashed region is excluded with the same confidence. The lower limits of the confidence intervals are all at null GW rate, but one per each type of search (galactic center and blind). These detections can, however, be explained as expected false alarms (see previous section and Appendix C) and do not affect the upper limits shown in the figures.

The upper bounds set by the network show in a few cases higher GW rates at higher thresholds than at lower thresholds (see Appendix C). This happens for the same reason why Figs. 6 and 7 may show increasing event rates and timing errors as H_t increases. In these cases, we chose to consider the most stringent upper bound value, on the basis of the fact that an upper limit computed at some threshold is also valid for any higher value of the threshold—as already remarked. This choice introduces a marginal bias on the stated coverage close to the plotted upper bounds.

The results of the blind search, Fig. 13, show a flat upper limit on the GW rate at high search thresholds, $H_t > 10^{-20} \text{ Hz}^{-1}$, where no coincidences have been found. This rate is determined by the *total* observation time of the network at those search thresholds, T_{obs} , and takes into account the conservative false dismissal of the time coincidence search. Specifically, the rate is given by $F/(T_{\text{obs}} \text{ C.L.}_c)$, where C.L._c is the confidence level of the time coincidence search procedure, $\text{C.L.}_c = 0.95$ for the data plotted, and the factor F depends on the required coverage, $F = 3.6$ for 0.95 probability. The confidence intervals on the rate widen at intermediate search thresholds mainly because of the presence of accidental coincidences. At $H_t \leq 3 \times 10^{-21} \text{ Hz}^{-1}$ the upper limit sharply increases because of the corresponding cutoff on the observation time. The results referred to the galactic center direction, Fig. 14, show a similar behavior, smoothed by the effect of the modulation of the directional sensitivity of the detectors. The relevant data are also tabulated in Appendix C.

C. Final remarks

The reported results refer to the GWs detected by the observatory, that is to say to the GWs present as coincidences in the IGEC exchanged data during the 1997–2000 observation time. In order to extend these results to the flux of GWs crossing Earth, one should take into account the actual efficiency of detection, which also depends on the specific model of the GW source, in particular on the GW amplitude distribution and rate. However, this goes beyond

the scope of the present paper. Here we set conservative detection efficiencies of the data analysis procedures.

The main progresses over the first IGEC analysis [12] rely on the optimization with respect to amplitude and direction of the GWs, on the balance between false dismissal probability and false alarm background, on the assessment of the statistical coverage of the upper limits and on the more extended observation time. The recent findings from the NAUTILUS and EXPLORER 2001 data [26] cannot be compared with the results of the analysis presented in this paper, as they relate to detectors runs with higher sensitivity.

We remind the reader once more that we are giving to the confidence intervals a frequentist statistical interpretation: they are determined to the best of our knowledge in order to include the actual value of the detected GW rate with a relative frequency given *on average* by the chosen coverage. The method and the likelihood from which the confidence intervals are computed are described in Sec. III E. An alternative approach based on the Bayesian framework can be followed for the data analysis. Section III E gives all the necessary information, in particular the most credible intervals assuming a uniform prior. These credible intervals would result similar to the ones we presented, but the value for their confidence and its interpretation would be different. For instance, the presented confidence intervals with 90% coverage would also be the most credible intervals with degree of belief of 94%, but different priors can be used as well.

IGEC amplitude data are in terms of the Fourier component H of the strain amplitude h of the GW burst signal. The relation between h and H depends on the specific model of signal shape. For instance, for a signal consisting of one sinusoidal cycle of 1-ms period $h \approx (2 \times 10^3 \text{ Hz}) \times H$. For such a source located at the galactic center and emitting isotropically, the estimated mass converted in GWs would be $\sim 0.01 M_{\odot} \times (H/1.5 \times 10^{-21} \text{ s})^2$.

The exchanged IGEC data do not allow the measurement of the light travel time of GW signals among the detector sites. In particular, past IGEC observations cannot resolve the GW direction. This capability will be achieved when upgraded detectors will demonstrate wider sensitivity bandwidths, much greater than 10 Hz and will implement signal acquisition and filtering ensuring submillisecond time resolution [23]. In fact, under these conditions, we expect that the overall uncertainties in estimated arrival time of the events will be much smaller than the light travel time between detector sites. Progress in this respect has been recently achieved [27] and is expected for the next runs of bar detectors [27,28].

ACKNOWLEDGMENTS

We wish to acknowledge the assistance of G. Maron and M. Biasotto, who set up the Linux PC farm used for the most intensive computations at INFN–Laboratori Nazionali di Legnaro. We are indebted to A. Colombo, M. Lollo, and G. Soranzo for their skilled technical help during the set up and operation of the GW detector AURIGA. This work has been partially funded by a grant COFIN 2000 from the Italian

MIUR. The work at LSU was funded by the National Science Foundation and by LSU. NIOBE was supported by the Australian Research Council.

APPENDIX A: TIME SERIES AND CORRELOGRAMS

Given two uniform and uncorrelated random point processes $\{t_1^i\}_{i \in \mathbb{N}}$ and $\{t_2^i\}_{i \in \mathbb{N}}$, the set of ordered time differences $\{\Delta^{ij} = t_1^i - t_2^j\}_{i_1 > i_2}$ between all possible pairs is described by a uniform distribution. This can be displayed by projecting all values in $\{\Delta^{ij}\}$ onto a histogram. The bin content is the *total* number of points of the original process $\{t_2^i\}_{i \in \mathbb{N}}$ that fall within a range (equal to the bin size) at a specified time lag from each of the points in the series $\{t_1^i\}_{i \in \mathbb{N}}$. As the two series are independent, this number is a Poisson variable, and its average value is bilinear in the number of events in $\{t_1^i\}_{i \in \mathbb{N}}$ and $\{t_2^i\}_{i \in \mathbb{N}}$. We call the histogram of generalized delays between points from different series a *cross correlogram* and a *self-correlogram* if $t_1^i = t_2^i$.

This representation has several advantages over a straightforward simple histogram of the time delays between *successive* points when it is applied to a Poisson point process. A simple time delay histogram describes the first order statistics and, for a perfectly homogeneous Poisson point process, would be fit by an exponential density function. However, this no longer holds true if the rate of the point process varies with time. In addition, any phase correlation at time lags longer than the average time separation is smeared out and not easily identified. A self-correlogram, on the other hand, retains much more information about the autocorrelation of the time series and is quite insensitive to fluctuations in the rate of the point process that occur on time scales longer than the range of the correlogram.

For instance, consider a nonhomogeneous Poisson point process, with a rate λ_1 for the first half of the time and a rate λ_2 for the other half. Its first order delay histogram is the sum of two different exponential distributions, while the self-correlogram is still flat (being the sum of two flat distributions). If on top of the random process we add a periodic series with constant rate $\lambda_p \ll \lambda_1, \lambda_2$, then it would be barely discernible in the first order histogram, while in the self-correlogram it would appear as a sharp peak at $1/\lambda_p$.

The cross correlation of two time series is related to the expected background due to accidental coincidences. If a bin of the cross correlogram has width dt and is centered at time lag Δt , then the counts inside this bin are proportional to the number of coincidences one would find after a time shift of one series by $\pm \Delta t$ and with time window aperture dt .

When the cross correlogram is not flat in a certain range of lags, this means that the statistics of the estimated background coincidence counts is not Poisson. Deviations from flatness would suggest a correlation of the rate of the point processes, either because of a common drive acting on more than one detector or because of different local signals, but with the same periodic characteristics. A similar feature

could also be caused by a border effect due to the time fragmentation of the data series.

APPENDIX B: TESTING COINCIDENCES AND FALSE DISMISSAL

In order to check if event times and amplitudes in different detectors are consistent with a common GW signal, we use the Bienaymè's inequality [29].

We recall that for a random variable x with mean η , the absolute value of the residual of x with respect to η is greater than ε with probability P , given by

$$P\{|x - \eta| \geq \varepsilon\} \leq \frac{E\{|x - \eta|^n\}}{\varepsilon^n}, \quad (\text{B1})$$

where $E\{|x - \eta|^n\}$ is the n th absolute central moment of x . Tchebyscheff's inequality is a special case for $n=2$. This inequality holds true for any statistics of x , as long as the moments exist.

When testing that η is the mean value, P is the conservative probability of false dismissal, i.e., of rejecting the hypothesis even though it is true. Concerning our analysis, we invert this inequality to compute ε given P , choosing the most convenient order n . Here ε can be conveniently expressed in terms of the standard deviation and a nondimensional multiplier, i.e., $\varepsilon = k\sigma$.

The IGEC exchanged data provide the variance of the estimated arrival time of the events as well as the central moments of second and fourth order of the amplitude noise distribution. To test the consistency of two values measured with different detectors we apply Bienaymè's inequality to the random variable $x_i - x_j$, which, in the case of events generated by the same GW excitation, has a zero mean, variance $\mu_{ij}^{(2)} \equiv \sigma_{ij}^2 \equiv \sigma_i^2 + \sigma_j^2$, and fourth moment $\mu_{ij}^{(4)} \equiv \mu_i^{(4)} + \mu_j^{(4)} + 6\sigma_i^2\sigma_j^2$, σ_i^2 and $\mu_i^{(4)}$ being the second and fourth order moments of the i th detector. Then, Eq. (B1) reduces to $P\{|x_i - x_j| \geq k\sigma_{ij}\} \leq k^{-n} \mu_{ij}^{(n)} / \sigma_{ij}^n$ and the coincidence test $|x_i - x_j| < k\sigma_{ij}$ is passed with the required maximum false dismissal probability P if we set $k = \sqrt[n]{(\mu_{ij}^{(n)} / \sigma_{ij}^n) / P}$, where the order n is used, which gives the most stringent check (given that moments of order $n > 2$ are available).

Regarding the value of the false dismissal P , there is an optimal choice to maximize the chances of GW detection. The value P_T used for comparison of event times, Eqs. (3) and (4), was chosen in order to balance between the conservative probability of detection of a GW coincidence, $1 - P_T$, and the related accidentals, whose number is proportional to the time window used for the coincidence search and therefore to $P_T^{-1/2}$. High values for P_T make the coincidence search less efficient, since its efficiency decreases more rapidly than the related background. On the contrary, setting P_T significantly below 5% has the drawback of gaining too little in terms of detection probability, while increas-

ing significantly the expected false alarms and their fluctuations. The choice $P_T=30\%$ would maximize precisely the ratio of the (conservative) detection efficiency and the corresponding number of accidental coincidences. However, what one should really care is the uncertainty due to Poisson fluctuations of the background rather than the average background itself. The contribution of these fluctuations when setting a confidence interval depends in a weaker way on P_T (approximately it is given by the square root of the average background). In the end, this would favor lower values for P_T , and the optimal choice is expected to be around 5%–10%. These expectations were confirmed by drawing the final results for different choices of P_T .

APPENDIX C: ANALYTIC TABLES OF COINCIDENCE COUNTS AND BACKGROUND ESTIMATES

In the following the reader can find more detailed information on the many analyses performed in this IGEC search. These trials differ for the directional search (none in Table II, optimization for the galactic center direction in Table III), for the investigated values of the GW amplitude threshold H_t and for the configurations of the network (there where at most 18 disjoint choices of detectors, plus the *total* lines, which synthesize the results of all configurations at the same threshold). For each trial we report the observation time, the corresponding coincidence counts and the background estimates. From these data and assuming that the bursts can be modeled as a Poisson point process, we compute the confidence intervals on the average number of GW bursts that possibly occurred within that time span (see Sec. III E). They are reported in the last two columns of the tables for two different values of the minimum coverage: namely, 90% and 95%.

Almost all of the computed confidence intervals cover the null result and therefore, at first glance, there is no strong evidence for GW detection. In order to be quantitative in this conclusion, we should undergo the not-so-easy task of estimating how many *false detections* we should expect in the tables. To do this, one has to consider the exact coverage of the confidence intervals for the specific case of no GW present in the data, rather than the stated conservative coverage, which is the minimum ensured coverage over any possible number of detected GWs. Second, one must also understand which lines in the tables are really independent and which ones are not.

As already remarked in Sec. IV A, the false alarm probability is much smaller than the conservative false dismissal. Considering the results on the whole, the number of detections found are in agreement with the false detections, predicted by summing up the expected false alarm probability of the hundreds of lines in the tables. We must be careful in drawing the conclusions, because the trials we are summing on are not completely independent. The following remarks help to get an idea of the degree of correlation among different lines in the tables.

(1) The configurations of detectors at the same search

threshold H_t in each table are independent, since they refer to mutually disjoint time spans.

(2) Moving toward high H_t , as soon as no coincidences are found and the observation time saturates to 100%, the results of each configuration do not depend anymore on H_t (for this reason we simplified the Table II at high H_t).

(3) The correlation among outcomes found at different amplitudes can be anything from zero to one. For instance, in Table II, stepping from 3.16 to $3.55 \times 10^{-20} \text{ Hz}^{-1}$ the total coincidence count is the same, $N_c=8$, but only 2 are in common.

(4) The correlation between the single configuration outcomes and the related *total* line can also vary, depending on the relative weight of the configurations in the sum. In case the total background counts are mostly due to a particular configuration, then the *total* is quite correlated with it, and therefore the total does not add much information. On the other hand, when a few expected total counts are spread in a balanced way among all configurations, then each of them may well end up showing a coincidence even if its specific background is low. These configurations count as many independent trials. Therefore, one should not make the mistake of selecting just those where a coincidence was found, because this would lead to a biased result. Instead, only the *total* line for that threshold should be considered in this case.

For all these reasons, the sparse hints of detection that can be found here and there in the tables have to be criticized from a statistical point of view. In particular, we shall discuss two specific cases in more detail.

The only positive result in a *total* line of Table II is at $H_t=3.98 \times 10^{-21} \text{ Hz}^{-1}$ and seems to confirm the detection suggested by the line EX-NI at the same amplitude. However, when correctly computing the conditioned probability that the *total* line is positive when $N_c(\text{EX-NI})=14$ is observed, we find it is as high as 54% at 95% coverage. Therefore we shall not claim a detection for this *total* line more than we would because of the single EX-NI result, and we are already aware of its small significance, considering the overall number of expected false detections over the single configurations.

In Table III the only detection are at $H_t=3.98 \times 10^{-21} \text{ Hz}^{-1}$: two detections at different configurations for 0.9 coverage and a detection at the *total* line for both 0.9 and 0.95 coverage. In order to compute the probability of getting a similar result by chance, we devised an empirical method [30] based on the information available from the time shifts estimates of the accidental coincidences (see Sec. III D). We built 1000 independent tables of results obtained from the samples of time shifted data, and we used the resulting statistics of detections as reference for the false alarms. The overall number of detections confirm the predictions reported in Sec. IV A. Moreover, the false alarm probability to show detections in at least one *total* line is 0.55 and 0.33 for 0.9 and 0.95 coverages, respectively. The probability of getting at least two detections at the same threshold value is 0.15 at 0.9 coverage. All probabilities are therefore well in agreement with no GW detection.

TABLE II. Results of the time coincidence search analysis for all the disjoint configurations of detectors whose observation time has been greater than 1 day. No directional search has been implemented. The coincidence search has been performed with a conservative false dismissal of 5%. The estimated average background \bar{N}_b $^{5\%}_{95\%}$ is reported together with its uncertainty, given either as 5% and 95% percentiles or as an 90% upper bound. When followed by the symbol *, the bound has to be read as a conservative upper limit (the actual upper bound is lower). Where the symbol—appears, there is no available estimate of the average background, though it does not affect the related confidence intervals because in these cases there were no found coincidences. For each search threshold H_t , the bottom *total* line summarizes the results, and is obtained by summing over all configurations the observation time T_{obs} , the number of coincidences N_c , and the background \bar{N}_b $^{5\%}_{95\%}$. In the last two columns, the confidence intervals on the average number of detected GWs are reported for 90% and 95% conservative coverage. Above the search threshold value $3 \times 10^{-20} \text{ Hz}^{-1}$ the results do not change.

$H_t \times 10^{21}$ (Hz^{-1})	config	T_{obs} (days)	N_c	\bar{N}_b $^{5\%}_{95\%}$	confidence interval	
					90%	95%
2.00	AU-NA	4.2	0	$0.4^{+0.034}_{-0.035}$	0–2.9	0–3.6
2.24	AU-NA	6.9	0	$0.4^{+0.033}_{-0.033}$	0–2.9	0–3.6
2.51	AU-NA	10.9	1	$0.5^{+0.036}_{-0.037}$	0–4.2	0–5
2.82	AL-NA	53.7	8	$7.9^{+0.15}_{-0.15}$	0–7.3	0–8.6
	AL-AU	38.9	2	$2.9^{+0.089}_{-0.089}$	0–4.3	0–5.2
	AU-NA	12.0	1	$0.6^{+0.04}_{-0.041}$	0–4.1	0–5
	AL-AU-NA	5.9	0	$4.9^{+3.4}_{-3.8} \times 10^{-4}$	0–2.9	0–3.6
	EX-NA	1.7	0	$0.2^{+0.023}_{-0.024}$	0–2.9	0–3.6
	AU-EX	1.6	0	$0.3^{+0.03}_{-0.03}$	0–2.9	0–3.6
	<i>total</i>	113.7	11	$12_{\pm 0.18}$	0–7.6	0–9
3.16	AL-NA	165.6	4	$3.6^{+0.099}_{-0.099}$	0–5.9	0–7
	AL-AU	115.7	2	$1.8^{+0.069}_{-0.07}$	0–4.7	0–5.7
	AL-AU-NA	24.6	0	$3.9^{+3}_{-3.4} \times 10^{-4}$	0–2.9	0–3.6
	AL-EX	6.5	0	$0.3^{+0.028}_{-0.029}$	0–2.9	0–3.6
	AU-EX	5.4	0	$0.9^{+0.049}_{-0.049}$	0–2.9	0–3.6
	AL-AU-EX	3.1	0	$2.9^{+2.5}_{-2.9} \times 10^{-4}$	0–2.9	0–3.6
	EX-NI	2.9	1	$1.5^{+0.064}_{-0.065}$	0–3.8	0–4.6
	EX-NA	2.7	1	$0.5^{+0.036}_{-0.037}$	0–4.2	0–5
	AU-NA	1.8	0	$6.1^{+1.3}_{-1.3} \times 10^{-2}$	0–2.9	0–3.6
	AL-AU-NI	1.2	0	$<1.8 \times 10^{-4} *$	0–2.9	0–3.6
	AL-NI	1.0	0	$4.8^{+1.1}_{-1.2} \times 10^{-2}$	0–2.9	0–3.6
	<i>total</i>	330.3	8	$8.7_{\pm 0.15}$	0–6.8	0–8.1
3.55	AL-NA	180.3	0	$0.5^{+0.037}_{-0.037}$	0–2.9	0–3.6
	AL-AU	120.1	0	$8.1^{+1.5}_{-1.5} \times 10^{-2}$	0–2.9	0–3.6
	AL-AU-NA	28.3	0	$2.9^{+2.5}_{-2.9} \times 10^{-4}$	0–2.9	0–3.6
	AL-EX	14.4	2	$7.6^{+1.4}_{-1.5} \times 10^{-2}$	0.25–6.1	0.15–7
	AU-EX	10.4	1	$0.9^{+0.05}_{-0.051}$	0–4	0–4.8
	EX-NI	8.8	3	$4.1^{+0.11}_{-0.11}$	0–4.7	0–5.7
	AL-AU-EX	8.0	0	$<1.8 \times 10^{-4} *$	0–2.9	0–3.6
	AL-AU-NI	4.5	0	$<1.8 \times 10^{-4} *$	0–2.9	0–3.6
	EX-NA	4.4	2	$1.2^{+0.058}_{-0.058}$	0–5.1	0–6
	AU-NA	2.3	0	$5.1^{+1.2}_{-1.2} \times 10^{-2}$	0–2.9	0–3.6
	AL-NI	2.3	0	$1.2^{+0.55}_{-0.059} \times 10^{-2}$	0–2.9	0–3.6
	AU-NI	1.5	0	$0.1^{+0.019}_{-0.02}$	0–2.9	0–3.6
	AL-EX-NA	1.4	0	$<1.8 \times 10^{-4} *$	0–2.9	0–3.6
	<i>total</i>	386.6	8	$7.2_{\pm 0.14}$	0–7.7	0–9
	3.75	AL-NA	186.6	0	$0.3^{+0.028}_{-0.028}$	0–2.9
AL-AU		117.9	0	$2.4^{+0.78}_{-0.83} \times 10^{-2}$	0–2.9	0–3.6
AL-AU-NA		28.9	0	$<1.8 \times 10^{-4} *$	0–2.9	0–3.6

TABLE II. (*Continued*).

$H_t \times 10^{21}$ (Hz^{-1})	config	T_{obs} (days)	N_c	\bar{N}_b ^{5%} _{95%}	confidence interval	
					90%	95%
	AL-EX	19.7	0	$5.1^{+1.2}_{-1.2} \times 10^{-2}$	0–2.9	0–3.6
	EX-NI	13.7	6	$6.2^{+0.13}_{-0.13}$	0–6.4	0–7.6
	AU-EX	12.3	1	$0.5^{+0.038}_{-0.038}$	0–4.2	0–5
	AL-AU-EX	11.1	0	$< 3.3 \times 10^{-4}$	0–2.9	0–3.6
	EX-NA	5.6	2	$1.6^{+0.066}_{-0.067}$	0–4.8	0–5.8
	AL-AU-NI	5.6	0	$< 1.8 \times 10^{-4} *$	0–2.9	0–3.6
	AL-NI	3.3	0	$1.1^{+0.52}_{-0.56} \times 10^{-2}$	0–2.9	0–3.6
	AL-EX-NA	2.8	0	$< 1.8 \times 10^{-4} *$	0–2.9	0–3.6
	AU-NA	2.4	0	$3.4^{+0.94}_{-0.98} \times 10^{-2}$	0–2.9	0–3.6
	AU-NI	2.0	0	$0.1^{+0.018}_{-0.018}$	0–2.9	0–3.6
	AL-AU-EX-NA	1.8	0	—	0–2.9	0–3.6
	<i>total</i>	413.4	9	$8.9_{\pm 0.16}$	0–7.6	0–8.9
3.98	AL-NA	191.9	0	$0.3^{+0.027}_{-0.027}$	0–2.9	0–3.6
	AL-AU	109.0	0	$1.2^{+0.55}_{-0.59} \times 10^{-2}$	0–2.9	0–3.6
	AL-AU-NA	29.4	0	$< 1.8 \times 10^{-4} *$	0–2.9	0–3.6
	AL-EX	26.3	0	$3^{+0.88}_{-0.92} \times 10^{-2}$	0–2.9	0–3.6
	EX-NI	20.1	14	$7.6^{+0.14}_{-0.14}$	0.6–14	0.013–16
	AL-AU-EX	14.0	0	$< 1.8 \times 10^{-4} *$	0–2.9	0–3.6
	AU-EX	13.4	2	$0.3^{+0.03}_{-0.031}$	0–5.8	0–6.7
	AL-AU-NI	11.2	0	$< 1.8 \times 10^{-4} *$	0–2.9	0–3.6
	EX-NA	7.2	3	$3.0^{+0.09}_{-0.09}$	0–5.2	0–6.2
	AL-EX-NA	4.8	0	$< 1.8 \times 10^{-4} *$	0–2.9	0–3.6
	AL-NI	4.7	0	$1.5^{+0.61}_{-0.66} \times 10^{-2}$	0–2.9	0–3.6
	AL-AU-EX-NA	2.8	0	—	0–2.9	0–3.6
	AU-NI	2.5	0	$5.4^{+1.2}_{-1.2} \times 10^{-2}$	0–2.9	0–3.6
	AU-NA	2.4	0	$2.8^{+0.85}_{-0.89} \times 10^{-2}$	0–2.9	0–3.6
	AU-EX-NI	1.8	0	$1.1^{+0.51}_{-0.55} \times 10^{-3}$	0–2.9	0–3.6
	AL-AU-EX-NI	1.4	0	—	0–2.9	0–3.6
	<i>total</i>	442.7	19	$11_{\pm 0.18}$	0.75–17	0.034–18
4.47	AL-NA	199.8	0	$0.2^{+0.022}_{-0.023}$	0–2.9	0–3.6
	AL-AU	99.6	0	$8^{+4.4}_{-4.8} \times 10^{-3}$	0–2.9	0–3.6
	AL-EX	39.1	0	$3.8^{+0.99}_{-1} \times 10^{-2}$	0–2.9	0–3.6
	EX-NI	35.5	15	$10.5^{+0.17}_{-0.17}$	0–12	0–14
	AL-AU-NA	29.6	0	$< 1.8 \times 10^{-4} *$	0–2.9	0–3.6
	AL-AU-EX	18.2	0	$< 1.8 \times 10^{-4} *$	0–2.9	0–3.6
	AU-EX	14.2	0	$0.1^{+0.017}_{-0.018}$	0–2.9	0–3.6
	EX-NA	13.1	10	$9.9^{+0.16}_{-0.16}$	0–7.9	0–9.2
	AL-AU-NI	12.1	0	$< 1.8 \times 10^{-4} *$	0–2.9	0–3.6
	AL-EX-NA	11.0	0	$< 1.8 \times 10^{-4} *$	0–2.9	0–3.6
	AL-NI	5.5	0	$< 1.8 \times 10^{-3} *$	0–2.9	0–3.6
	AL-AU-EX-NA	5.1	0	—	0–2.9	0–3.6
	AL-AU-EX-NI	4.4	0	—	0–2.9	0–3.6
	AU-NI	3.7	0	$3.7^{+0.98}_{-1} \times 10^{-2}$	0–2.9	0–3.6
	AU-EX-NI	3.2	0	$< 1.8 \times 10^{-4} *$	0–2.9	0–3.6
	AU-NA	2.3	0	$6^{+3.8}_{-4.2} \times 10^{-3}$	0–2.9	0–3.6
	AL-EX-NI	2.3	0	$< 1.8 \times 10^{-4} *$	0–2.9	0–3.6
	<i>total</i>	498.9	25	$21_{\pm 0.24}$	0–14	0–16
5.01	AL-NA	203.2	0	$0.1^{+0.018}_{-0.018}$	0–2.9	0–3.6
	AL-AU	92.0	0	$4^{+3}_{-3.4} \times 10^{-3}$	0–2.9	0–3.6
	AL-EX	56.4	0	$7.1^{+1.4}_{-1.4} \times 10^{-2}$	0–2.9	0–3.6

TABLE II. (*Continued*).

$H_t \times 10^{21}$ (Hz^{-1})	config	T_{obs} (days)	N_c	\bar{N}_b ^{5%} _{95%}	confidence interval	
					90%	95%
	EX-NI	47.1	7	$6.8^{+0.14}_{-0.14}$	0–7	0–8.2
	AL-AU-NA	29.1	0	$<1.8 \times 10^{-4}*$	0–2.9	0–3.6
	EX-NA	25.5	23	$22.4^{+0.25}_{-0.25}$	0–11	0–13
	AL-AU-EX	23.5	0	$<1.8 \times 10^{-4}*$	0–2.9	0–3.6
	AL-EX-NA	20.2	0	$<1.8 \times 10^{-4}*$	0–2.9	0–3.6
	AU-EX	15.7	0	$4.4^{+1.1}_{-1.1} \times 10^{-2}$	0–2.9	0–3.6
	AL-AU-NI	11.2	0	$<1.8 \times 10^{-4}*$	0–2.9	0–3.6
	AL-AU-EX-NA	7.3	0	—	0–2.9	0–3.6
	AL-AU-EX-NI	6.3	0	—	0–2.9	0–3.6
	AL-NI	5.5	0	$<1.8 \times 10^{-3}*$	0–2.9	0–3.6
	AU-NI	5.2	0	$2.5^{+0.8}_{-0.84} \times 10^{-2}$	0–2.9	0–3.6
	AU-EX-NI	4.2	0	$<1.8 \times 10^{-4}*$	0–2.9	0–3.6
	AL-EX-NI	3.8	0	$<1.8 \times 10^{-4}*$	0–2.9	0–3.6
	AU-NA	2.3	0	$<1.8 \times 10^{-3}*$	0–2.9	0–3.6
	<i>total</i>	558.6	30	$29_{\pm 0.28}$	0–13	0–15
5.62	AL-NA	201.6	0	$8.4^{+1.5}_{-1.5} \times 10^{-2}$	0–2.9	0–3.6
	AL-AU	85.3	0	$<1.8 \times 10^{-3}$	0–2.9	0–3.6
	AL-EX	71.5	0	$0.1^{+0.019}_{-0.02}$	0–2.9	0–3.6
	EX-NI	55.2	4	$6.7^{+0.13}_{-0.13}$	0–4.7	0–5.7
	EX-NA	36.9	20	$19.4^{+0.23}_{-0.23}$	0–11	0–12
	AL-EX-NA	31.2	0	$<1.8 \times 10^{-4}*$	0–2.9	0–3.6
	AL-AU-NA	28.7	0	$<1.8 \times 10^{-4}*$	0–2.9	0–3.6
	AL-AU-EX	26.9	0	$<1.8 \times 10^{-4}*$	0–2.9	0–3.6
	AU-EX	17.0	0	$1.6^{+0.63}_{-0.68} \times 10^{-2}$	0–2.9	0–3.6
	AL-AU-NI	11.2	0	$<1.8 \times 10^{-4}*$	0–2.9	0–3.6
	AL-NI	10.2	0	$<1.8 \times 10^{-3}*$	0–2.9	0–3.6
	AL-AU-EX-NA	9.0	0	—	0–2.9	0–3.6
	AL-AU-EX-NI	8.3	0	—	0–2.9	0–3.6
	AU-NI	6.2	0	$1.7^{+0.65}_{-0.7} \times 10^{-2}$	0–2.9	0–3.6
	AU-EX-NI	5.6	0	$<1.8 \times 10^{-4}*$	0–2.9	0–3.6
	AL-EX-NI	5.0	0	$<1.8 \times 10^{-4}*$	0–2.9	0–3.6
	AU-NA	2.4	0	$<1.8 \times 10^{-3}*$	0–2.9	0–3.6
	<i>total</i>	612.4	24	$26_{\pm 0.27}$	0–9.8	0–12
6.31	AL-NA	198.4	0	$7.4^{+1.4}_{-1.4} \times 10^{-2}$	0–2.9	0–3.6
	AL-EX	84.5	0	$0.1^{+0.017}_{-0.018}$	0–2.9	0–3.6
	AL-AU	80.4	0	$<1.8 \times 10^{-3}$	0–2.9	0–3.6
	EX-NI	61.9	4	$6.1^{+0.13}_{-0.13}$	0–4.9	0–5.9
	EX-NA	45.1	10	$12.8^{+0.19}_{-0.19}$	0–6.5	0–7.8
	AL-EX-NA	41.0	0	$<1.8 \times 10^{-4}*$	0–2.9	0–3.6
	AL-AU-EX	29.0	0	$<1.8 \times 10^{-4}*$	0–2.9	0–3.6
	AL-AU-NA	27.2	0	$<1.8 \times 10^{-4}*$	0–2.9	0–3.6
	AU-EX	16.0	0	$8^{+4.4}_{-4.8} \times 10^{-3}$	0–2.9	0–3.6
	AL-NI	12.8	0	$<3.4 \times 10^{-3}$	0–2.9	0–3.6
	AL-AU-NI	11.6	0	$<1.8 \times 10^{-4}*$	0–2.9	0–3.6
	AL-AU-EX-NA	11.2	0	—	0–2.9	0–3.6
	AL-AU-EX-NI	10.2	0	—	0–2.9	0–3.6
	AU-EX-NI	8.6	0	$<1.8 \times 10^{-4}*$	0–2.9	0–3.6
	AU-NI	6.9	0	$1.1^{+0.52}_{-0.56} \times 10^{-2}$	0–2.9	0–3.6
	AL-EX-NI	6.0	0	$<1.8 \times 10^{-4}*$	0–2.9	0–3.6

TABLE II. (*Continued*).

$H_t \times 10^{21}$ (Hz^{-1})	config	T_{obs} (days)	N_c	\bar{N}_b $^{5\%}_{95\%}$	confidence interval	
					90%	95%
	AU-NA	2.3	0	$< 1.8 \times 10^{-3}*$	0–2.9	0–3.6
	<i>total</i>	653.0	14	$19_{\pm 0.23}$	0–6.7	0–8.1
7.08	AL-NA	193.8	0	$5.5^{+1.2}_{-1.2} \times 10^{-2}$	0–2.9	0–3.6
	AL-EX	96.4	0	$0.1^{+0.018}_{-0.018}$	0–2.9	0–3.6
	AL-AU	76.9	0	$< 1.8 \times 10^{-3}*$	0–2.9	0–3.6
	EX-NI	65.3	3	$3.4^{+0.096}_{-0.096}$	0–5	0–6
	EX-NA	49.4	6	$6.0^{+0.13}_{-0.13}$	0–6.5	0–7.7
	AL-EX-NA	48.2	0	$< 1.8 \times 10^{-4}*$	0–2.9	0–3.6
	AL-AU-EX	32.0	0	$< 1.8 \times 10^{-4}*$	0–2.9	0–3.6
	AL-AU-NA	26.1	0	$< 1.8 \times 10^{-4}*$	0–2.9	0–3.6
	AU-EX	16.5	0	$< 1.8 \times 10^{-3}$	0–2.9	0–3.6
	AL-NI	12.9	0	$< 3.4 \times 10^{-3}$	0–2.9	0–3.6
	AL-AU-EX-NA	12.6	0	—	0–2.9	0–3.6
	AL-AU-NI	11.1	0	$< 1.8 \times 10^{-4}*$	0–2.9	0–3.6
	AL-AU-EX-NI	10.9	0	—	0–2.9	0–3.6
	AU-EX-NI	9.3	0	$< 1.8 \times 10^{-4}*$	0–2.9	0–3.6
	AL-EX-NI	6.8	0	$< 1.8 \times 10^{-4}*$	0–2.9	0–3.6
	AU-NI	6.5	0	$3^{+2.6}_{-3} \times 10^{-3}$	0–2.9	0–3.6
	AU-NA	2.1	0	$< 1.8 \times 10^{-3}*$	0–2.9	0–3.6
<i>total</i>		676.8	9	$9.6_{\pm 0.16}$	0–7.2	0–8.5
7.94	AL-NA	189.2	0	$3.6^{+0.96}_{-1} \times 10^{-2}$	0–2.9	0–3.6
	AL-EX	106.1	0	$6.4^{+1.3}_{-1.3} \times 10^{-2}$	0–2.9	0–3.6
	AL-AU	74.4	0	$< 1.8 \times 10^{-3}*$	0–2.9	0–3.6
	EX-NI	68.2	6	$2.4^{+0.081}_{-0.081}$	0.12–9.3	0–10
	AL-EX-NA	54.3	0	$< 1.8 \times 10^{-4}*$	0–2.9	0–3.6
	EX-NA	51.6	2	$2.6^{+0.084}_{-0.084}$	0–4.4	0–5.3
	AL-AU-EX	34.8	0	$< 1.8 \times 10^{-4}*$	0–2.9	0–3.6
	AL-AU-NA	25.1	0	$< 1.8 \times 10^{-4}*$	0–2.9	0–3.6
	AU-EX	16.9	0	$< 1.8 \times 10^{-3}*$	0–2.9	0–3.6
	AL-AU-EX-NA	13.6	0	—	0–2.9	0–3.6
	AL-NI	12.7	0	$< 1.8 \times 10^{-3}*$	0–2.9	0–3.6
	AL-AU-EX-NI	11.3	0	—	0–2.9	0–3.6
	AL-AU-NI	10.8	0	$< 1.8 \times 10^{-4}*$	0–2.9	0–3.6
	AU-EX-NI	9.8	0	$< 1.8 \times 10^{-4}*$	0–2.9	0–3.6
	AL-EX-NI	7.1	0	$< 1.8 \times 10^{-4}*$	0–2.9	0–3.6
	AU-NI	6.0	0	$< 1.8 \times 10^{-3}$	0–2.9	0–3.6
	AU-NA	2.0	0	$< 1.8 \times 10^{-3}*$	0–2.9	0–3.6
<i>total</i>		694.3	8	$5.1_{\pm 0.12}$	0–9.2	0–11
8.91	AL-NA	187.5	0	$3.1^{+0.89}_{-0.94} \times 10^{-2}$	0–2.9	0–3.6
	AL-EX	110.6	0	$4.9^{+1.1}_{-1.2} \times 10^{-2}$	0–2.9	0–3.6
	AL-AU	73.8	0	$< 1.8 \times 10^{-3}*$	0–2.9	0–3.6
	EX-NI	69.5	2	$1.7^{+0.067}_{-0.067}$	0–4.8	0–5.7
	AL-EX-NA	56.8	0	$< 1.8 \times 10^{-4}*$	0–2.9	0–3.6
	EX-NA	52.5	2	$1.6^{+0.066}_{-0.067}$	0–4.8	0–5.8
	AL-AU-EX	35.8	0	$< 1.8 \times 10^{-4}*$	0–2.9	0–3.6
	AL-AU-NA	24.8	0	$< 1.8 \times 10^{-4}*$	0–2.9	0–3.6
	AU-EX	17.1	0	$4^{+3}_{-3.4} \times 10^{-3}$	0–2.9	0–3.6
	AL-AU-EX-NA	14.1	0	—	0–2.9	0–3.6
	AL-NI	12.7	0	$< 1.8 \times 10^{-3}*$	0–2.9	0–3.6
	AL-AU-EX-NI	11.4	0	—	0–2.9	0–3.6

TABLE II. (*Continued*).

$H_t \times 10^{21}$ (Hz^{-1})	config	T_{obs} (days)	N_c	\bar{N}_b ^{5%} _{95%}	confidence interval	
					90%	95%
	AL-AU-NI	10.7	0	$< 1.8 \times 10^{-4} *$	0–2.9	0–3.6
	AU-EX-NI	10.0	0	$< 1.8 \times 10^{-4} *$	0–2.9	0–3.6
	AL-EX-NI	7.2	0	$< 1.8 \times 10^{-4} *$	0–2.9	0–3.6
	AU-NI	5.9	0	$< 1.8 \times 10^{-3}$	0–2.9	0–3.6
	AU-NA	2.0	0	$< 1.8 \times 10^{-3} *$	0–2.9	0–3.6
	<i>total</i>	702.4	4	$3.4_{\pm 0.095}$	0–6	0–7.1
10.00	AL-NA	187.2	0	$2.4_{-0.83}^{+0.78} \times 10^{-2}$	0–2.9	0–3.6
	AL-EX	113.0	0	$4_{-1.1}^{+1} \times 10^{-2}$	0–2.9	0–3.6
	AL-AU	73.5	0	$< 1.8 \times 10^{-3} *$	0–2.9	0–3.6
	EX-NI	70.0	1	$1.0_{-0.053}^{+0.052}$	0–3.9	0–4.8
	AL-EX-NA	57.6	0	$< 1.8 \times 10^{-4} *$	0–2.9	0–3.6
	EX-NA	52.7	1	$1.2_{-0.057}^{+0.056}$	0–3.9	0–4.7
	AL-AU-EX	36.2	0	$< 1.8 \times 10^{-4} *$	0–2.9	0–3.6
	AL-AU-NA	24.7	0	$< 1.8 \times 10^{-4} *$	0–2.9	0–3.6
	AU-EX	17.1	0	$< 1.8 \times 10^{-3}$	0–2.9	0–3.6
	AL-AU-EX-NA	14.2	0	—	0–2.9	0–3.6
	AL-NI	12.7	0	$< 1.8 \times 10^{-3} *$	0–2.9	0–3.6
	AL-AU-EX-NI	11.4	0	—	0–2.9	0–3.6
	AL-AU-NI	10.7	0	$< 1.8 \times 10^{-4} *$	0–2.9	0–3.6
	AU-EX-NI	10.0	0	$< 1.8 \times 10^{-4} *$	0–2.9	0–3.6
	AL-EX-NI	7.2	0	$< 1.8 \times 10^{-4} *$	0–2.9	0–3.6
	AU-NI	5.9	0	$< 1.8 \times 10^{-3} *$	0–2.9	0–3.6
	AU-NA	2.0	0	$< 1.8 \times 10^{-3} *$	0–2.9	0–3.6
	<i>total</i>	706.4	2	$2.3_{\pm 0.078}$	0–4.5	0–5.4
11.22	AL-NA	187.1	0	$1.3_{-0.61}^{+0.57} \times 10^{-2}$	0–2.9	0–3.6
	AL-EX	113.7	0	$2.8_{-0.89}^{+0.85} \times 10^{-2}$	0–2.9	0–3.6
	AL-AU	73.6	0	$< 1.8 \times 10^{-3} *$	0–2.9	0–3.6
	EX-NI	70.1	0	$0.4_{-0.034}^{+0.034}$	0–2.9	0–3.6
	AL-EX-NA	57.8	0	$< 1.8 \times 10^{-4} *$	0–2.9	0–3.6
	EX-NA	52.9	1	$1.0_{-0.051}^{+0.051}$	0–4	0–4.8
	AL-AU-EX	36.3	0	$< 1.8 \times 10^{-4} *$	0–2.9	0–3.6
	AL-AU-NA	24.7	0	$< 1.8 \times 10^{-4} *$	0–2.9	0–3.6
	AU-EX	17.1	0	$1.7_{-0.7}^{+0.65} \times 10^{-2}$	0–2.9	0–3.6
	AL-AU-EX-NA	14.2	0	—	0–2.9	0–3.6
	AL-NI	12.7	0	$< 1.8 \times 10^{-3} *$	0–2.9	0–3.6
	AL-AU-EX-NI	11.4	0	—	0–2.9	0–3.6
	AL-AU-NI	10.6	0	$< 1.8 \times 10^{-4} *$	0–2.9	0–3.6
	AU-EX-NI	10.1	0	$< 1.8 \times 10^{-4} *$	0–2.9	0–3.6
	AL-EX-NI	7.2	0	$< 1.8 \times 10^{-4} *$	0–2.9	0–3.6
	AU-NI	5.8	0	$< 1.8 \times 10^{-3} *$	0–2.9	0–3.6
	AU-NA	2.0	0	$< 1.8 \times 10^{-3} *$	0–2.9	0–3.6
	<i>total</i>	707.7	1	$1.5_{\pm 0.063}$	0–3.8	0–4.6
12.59	AL-NA	187.1	0	$1.1_{-0.56}^{+0.52} \times 10^{-2}$	0–2.9	0–3.6
	AL-EX	113.7	0	$1.1_{-0.56}^{+0.52} \times 10^{-2}$	0–2.9	0–3.6
	AL-AU	73.6	0	$< 1.8 \times 10^{-3} *$	0–2.9	0–3.6
	EX-NI	70.2	0	$0.2_{-0.026}^{+0.025}$	0–2.9	0–3.6
	AL-EX-NA	57.8	0	$< 1.8 \times 10^{-4} *$	0–2.9	0–3.6
	EX-NA	52.9	0	$0.7_{-0.045}^{+0.044}$	0–2.9	0–3.6
	AL-AU-EX	36.4	0	$< 1.8 \times 10^{-4} *$	0–2.9	0–3.6
	AL-AU-NA	24.7	0	$< 1.8 \times 10^{-4} *$	0–2.9	0–3.6

TABLE II. (*Continued*).

$H_t \times 10^{21}$ (Hz ⁻¹)	config	T_{obs} (days)	N_c	\bar{N}_b ^{5%} _{95%}	confidence interval	
					90%	95%
	AU-EX	17.2	0	$1.6^{+0.63}_{-0.68} \times 10^{-2}$	0–2.9	0–3.6
	AL-AU-EX-NA	14.0	0	—	0–2.9	0–3.6
	AL-NI	12.7	0	$< 1.8 \times 10^{-3}*$	0–2.9	0–3.6
	AL-AU-EX-NI	11.4	0	—	0–2.9	0–3.6
	AL-AU-NI	10.6	0	$< 1.8 \times 10^{-4}*$	0–2.9	0–3.6
	AU-EX-NI	10.1	0	$< 1.8 \times 10^{-4}*$	0–2.9	0–3.6
	AL-EX-NI	7.2	0	$< 1.8 \times 10^{-4}*$	0–2.9	0–3.6
	AU-NI	5.8	0	$< 1.8 \times 10^{-3}*$	0–2.9	0–3.6
	AU-NA	2.0	0	$< 1.8 \times 10^{-3}*$	0–2.9	0–3.6
	<i>total</i>	707.8	0	$1_{\pm 0.053}$	0–2.9	0–3.6
14.12	AL-NA	187.1	0	$3^{+2.6}_{-3} \times 10^{-3}$	0–2.9	0–3.6
	AL-EX	113.7	0	$8^{+4.4}_{-4.8} \times 10^{-3}$	0–2.9	0–3.6
	AL-AU	73.6	0	$< 1.8 \times 10^{-3}*$	0–2.9	0–3.6
	EX-NI	70.2	0	$0.1^{+0.019}_{-0.019}$	0–2.9	0–3.6
	AL-EX-NA	57.8	0	$< 1.8 \times 10^{-4}*$	0–2.9	0–3.6
	EX-NA	52.9	0	$0.4^{+0.033}_{-0.033}$	0–2.9	0–3.6
	AL-AU-EX	36.4	0	$< 1.8 \times 10^{-4}*$	0–2.9	0–3.6
	AL-AU-NA	24.7	0	$< 1.8 \times 10^{-4}*$	0–2.9	0–3.6
	AU-EX	17.2	0	$< 1.8 \times 10^{-3}*$	0–2.9	0–3.6
	AL-AU-EX-NA	14.2	0	—	0–2.9	0–3.6
	AL-NI	12.7	0	$< 1.8 \times 10^{-3}*$	0–2.9	0–3.6
	AL-AU-EX-NI	11.4	0	—	0–2.9	0–3.6
	AL-AU-NI	10.6	0	$< 1.8 \times 10^{-4}*$	0–2.9	0–3.6
	AU-EX-NI	10.1	0	$< 1.8 \times 10^{-4}*$	0–2.9	0–3.6
	AL-EX-NI	7.2	0	$< 1.8 \times 10^{-4}*$	0–2.9	0–3.6
	AU-NI	5.8	0	$< 1.8 \times 10^{-3}*$	0–2.9	0–3.6
	AU-NA	2.0	0	$< 1.8 \times 10^{-3}*$	0–2.9	0–3.6
	<i>total</i>	707.9	0	$0.55_{\pm 0.038}$	0–2.9	0–3.6
15.85	AL-NA	187.1	0	$< 1.8 \times 10^{-3}$	0–2.9	0–3.6
	AL-EX	113.7	0	$6^{+3.8}_{-4.2} \times 10^{-3}$	0–2.9	0–3.6
	AL-AU	73.6	0	$< 1.8 \times 10^{-3}*$	0–2.9	0–3.6
	EX-NI	70.2	0	$6.9^{+1.3}_{-1.4} \times 10^{-2}$	0–2.9	0–3.6
	AL-EX-NA	57.8	0	$< 1.8 \times 10^{-4}*$	0–2.9	0–3.6
	EX-NA	52.9	0	$0.2^{+0.024}_{-0.024}$	0–2.9	0–3.6
	AL-AU-EX	36.4	0	$< 1.8 \times 10^{-4}*$	0–2.9	0–3.6
	AL-AU-NA	24.7	0	$< 1.8 \times 10^{-4}*$	0–2.9	0–3.6
	AU-EX	17.2	0	$< 1.8 \times 10^{-3}*$	0–2.9	0–3.6
	AL-AU-EX-NA	14.2	0	—	0–2.9	0–3.6
	AL-NI	12.7	0	$< 1.8 \times 10^{-3}*$	0–2.9	0–3.6
	AL-AU-EX-NI	11.4	0	—	0–2.9	0–3.6
	AL-AU-NI	10.6	0	$< 1.8 \times 10^{-4}*$	0–2.9	0–3.6
	AU-EX-NI	10.1	0	$< 1.8 \times 10^{-4}*$	0–2.9	0–3.6
	AL-EX-NI	7.2	0	$< 1.8 \times 10^{-4}*$	0–2.9	0–3.6
	AU-NI	5.8	0	$< 1.8 \times 10^{-3}*$	0–2.9	0–3.6
	AU-NA	2.0	0	$< 1.8 \times 10^{-3}*$	0–2.9	0–3.6
	<i>total</i>	707.9	0	$0.31_{\pm 0.028}$	0–2.9	0–3.6
17.78	AL-NA	187.1	0	$< 1.8 \times 10^{-3}*$	0–2.9	0–3.6
	AL-EX	113.7	0	$5^{+3.4}_{-3.8} \times 10^{-3}$	0–2.9	0–3.6
	AL-AU	73.6	0	$< 1.8 \times 10^{-3}*$	0–2.9	0–3.6
	EX-NI	70.2	0	$2.1^{+0.73}_{-0.77} \times 10^{-2}$	0–2.9	0–3.6

TABLE II. (*Continued*).

$H_t \times 10^{21}$ (Hz ⁻¹)	config	T_{obs} (days)	N_c	\bar{N}_b ^{5%} _{95%}	confidence interval	
					90%	95%
	AL-EX-NA	57.8	0	$< 1.8 \times 10^{-4} *$	0-2.9	0-3.6
	EX-NA	52.9	0	$0.1^{+0.017}_{-0.017}$	0-2.9	0-3.6
	AL-AU-EX	36.4	0	$< 1.8 \times 10^{-4} *$	0-2.9	0-3.6
	AL-AU-NA	24.7	0	$< 1.8 \times 10^{-4} *$	0-2.9	0-3.6
	AU-EX	17.2	0	$< 1.8 \times 10^{-3} *$	0-2.9	0-3.6
	AL-AU-EX-NA	14.2	0	—	0-2.9	0-3.6
	AL-NI	12.7	0	$< 1.8 \times 10^{-3} *$	0-2.9	0-3.6
	AL-AU-EX-NI	11.4	0	—	0-2.9	0-3.6
	AL-AU-NI	10.6	0	$< 1.8 \times 10^{-4} *$	0-2.9	0-3.6
	AU-EX-NI	10.1	0	$< 1.8 \times 10^{-4} *$	0-2.9	0-3.6
	AL-EX-NI	7.2	0	$< 1.8 \times 10^{-4} *$	0-2.9	0-3.6
	AU-NI	5.8	0	$< 1.8 \times 10^{-3} *$	0-2.9	0-3.6
	AU-NA	2.0	0	$< 1.8 \times 10^{-3} *$	0-2.9	0-3.6
	<i>total</i>	707.9	0	$0.15_{\pm 0.02}$	0-2.9	0-3.6
19.95	AL-NA	187.1	0	$< 1.8 \times 10^{-3} *$	0-2.9	0-3.6
	AL-EX	113.7	0	$4^{+3}_{-3.4} \times 10^{-3}$	0-2.9	0-3.6
	AL-AU	73.6	0	$< 1.8 \times 10^{-3} *$	0-2.9	0-3.6
	EX-NI	70.2	0	$7^{+4.1}_{-4.5} \times 10^{-3}$	0-2.9	0-3.6
	AL-EX-NA	57.8	0	$< 1.8 \times 10^{-4} *$	0-2.9	0-3.6
	EX-NA	52.9	0	$4.7^{+1.1}_{-1.1} \times 10^{-2}$	0-2.9	0-3.6
	AL-AU-EX	36.4	0	$< 1.8 \times 10^{-4} *$	0-2.9	0-3.6
	AL-AU-NA	24.7	0	$< 1.8 \times 10^{-4} *$	0-2.9	0-3.6
	AU-EX	17.2	0	$< 1.8 \times 10^{-3} *$	0-2.9	0-3.6
	AL-AU-EX-NA	14.2	0	—	0-2.9	0-3.6
	AL-NI	12.7	0	$< 1.8 \times 10^{-3} *$	0-2.9	0-3.6
	AL-AU-EX-NI	11.4	0	—	0-2.9	0-3.6
	AL-AU-NI	10.6	0	$< 1.8 \times 10^{-4} *$	0-2.9	0-3.6
	AU-EX-NI	10.1	0	$< 1.8 \times 10^{-4} *$	0-2.9	0-3.6
	AL-EX-NI	7.2	0	$< 1.8 \times 10^{-4} *$	0-2.9	0-3.6
	AU-NI	5.8	0	$< 1.8 \times 10^{-3} *$	0-2.9	0-3.6
	AU-NA	2.0	0	$< 1.8 \times 10^{-3} *$	0-2.9	0-3.6
	<i>total</i>	707.9	0	$7_{\pm 1.3} \times 10^{-2}$	0-2.9	0-3.6
22.39	AL-NA	187.1	0	$< 1.8 \times 10^{-3} *$	0-2.9	0-3.6
	AL-EX	113.7	0	$3^{+2.6}_{-3} \times 10^{-3}$	0-2.9	0-3.6
	AL-AU	73.6	0	$< 1.8 \times 10^{-3} *$	0-2.9	0-3.6
	EX-NI	70.2	0	$5^{+3.4}_{-3.8} \times 10^{-3}$	0-2.9	0-3.6
	AL-EX-NA	57.8	0	$< 1.8 \times 10^{-4} *$	0-2.9	0-3.6
	EX-NA	52.9	0	$1.8^{+0.67}_{-0.72} \times 10^{-2}$	0-2.9	0-3.6
	AL-AU-EX	36.4	0	$< 1.8 \times 10^{-4} *$	0-2.9	0-3.6
	AL-AU-NA	24.7	0	$< 1.8 \times 10^{-4} *$	0-2.9	0-3.6
	AU-EX	17.2	0	$< 1.8 \times 10^{-3} *$	0-2.9	0-3.6
	AL-AU-EX-NA	14.2	0	—	0-2.9	0-3.6
	AL-NI	12.7	0	$< 1.8 \times 10^{-3} *$	0-2.9	0-3.6
	AL-AU-EX-NI	11.4	0	—	0-2.9	0-3.6
	AL-AU-NI	10.6	0	$< 1.8 \times 10^{-4} *$	0-2.9	0-3.6
	AU-EX-NI	10.1	0	$< 1.8 \times 10^{-4} *$	0-2.9	0-3.6
	AL-EX-NI	7.2	0	$< 1.8 \times 10^{-4} *$	0-2.9	0-3.6
	AU-NI	5.8	0	$< 1.8 \times 10^{-3} *$	0-2.9	0-3.6
	AU-NA	2.0	0	$< 1.8 \times 10^{-3} *$	0-2.9	0-3.6
	<i>total</i>	707.9	0	$3.8_{\pm 0.93} \times 10^{-2}$	0-2.9	0-3.6

TABLE II. (*Continued*).

$H_t \times 10^{21}$ (Hz ⁻¹)	config	T_{obs} (days)	N_c	\bar{N}_b ^{5%} _{95%}	confidence interval	
					90%	95%
25.12	AL-NA	187.1	0	$< 1.8 \times 10^{-3} *$	0-2.9	0-3.6
	AL-EX	113.7	0	$3_{-3}^{+2.6} \times 10^{-3}$	0-2.9	0-3.6
	AL-AU	73.6	0	$< 1.8 \times 10^{-3} *$	0-2.9	0-3.6
	EX-NI	70.2	0	$4_{-3.4}^{+3} \times 10^{-3}$	0-2.9	0-3.6
	AL-EX-NA	57.8	0	$< 1.8 \times 10^{-4} *$	0-2.9	0-3.6
	EX-NA	52.9	0	$1.1_{-0.56}^{+0.52} \times 10^{-2}$	0-2.9	0-3.6
	AL-AU-EX	36.4	0	$< 1.8 \times 10^{-4} *$	0-2.9	0-3.6
	AL-AU-NA	24.7	0	$< 1.8 \times 10^{-4} *$	0-2.9	0-3.6
	AU-EX	17.2	0	$< 1.8 \times 10^{-3} *$	0-2.9	0-3.6
	AL-AU-EX-NA	14.2	0	—	0-2.9	0-3.6
	AL-NI	12.7	0	$< 1.8 \times 10^{-3} *$	0-2.9	0-3.6
	AL-AU-EX-NI	11.4	0	—	0-2.9	0-3.6
	AL-AU-NI	10.6	0	$< 1.8 \times 10^{-4} *$	0-2.9	0-3.6
	AU-EX-NI	10.1	0	$< 1.8 \times 10^{-4} *$	0-2.9	0-3.6
	AL-EX-NI	7.2	0	$< 1.8 \times 10^{-4} *$	0-2.9	0-3.6
	AU-NI	5.8	0	$< 1.8 \times 10^{-3} *$	0-2.9	0-3.6
	AU-NA	2.0	0	$< 1.8 \times 10^{-3} *$	0-2.9	0-3.6
<i>total</i>		707.9	0	$3_{\pm 0.81} \times 10^{-2}$	0-2.9	0-3.6
28.18	AL-NA	187.1	0	$< 1.8 \times 10^{-3} *$	0-2.9	0-3.6
	AL-EX	113.7	0	$3_{-3}^{+2.6} \times 10^{-3}$	0-2.9	0-3.6
	AL-AU	73.6	0	$< 1.8 \times 10^{-3} *$	0-2.9	0-3.6
	EX-NI	70.2	0	$3_{-3}^{+2.6} \times 10^{-3}$	0-2.9	0-3.6
	AL-EX-NA	57.8	0	$< 1.8 \times 10^{-4} *$	0-2.9	0-3.6
	EX-NA	52.9	0	$9_{-5.1}^{+4.7} \times 10^{-3}$	0-2.9	0-3.6
	AL-AU-EX	36.4	0	$< 1.8 \times 10^{-4} *$	0-2.9	0-3.6
	AL-AU-NA	24.7	0	$< 1.8 \times 10^{-4} *$	0-2.9	0-3.6
	AU-EX	17.2	0	$< 1.8 \times 10^{-3} *$	0-2.9	0-3.6
	AL-AU-EX-NA	14.2	0	—	0-2.9	0-3.6
	AL-NI	12.7	0	$< 1.8 \times 10^{-3} *$	0-2.9	0-3.6
	AL-AU-EX-NI	11.4	0	—	0-2.9	0-3.6
	AL-AU-NI	10.6	0	$< 1.8 \times 10^{-4} *$	0-2.9	0-3.6
	AU-EX-NI	10.1	0	$< 1.8 \times 10^{-4} *$	0-2.9	0-3.6
	AL-EX-NI	7.2	0	$< 1.8 \times 10^{-4} *$	0-2.9	0-3.6
	AU-NI	5.8	0	$< 1.8 \times 10^{-3} *$	0-2.9	0-3.6
	AU-NA	2.0	0	$< 1.8 \times 10^{-3} *$	0-2.9	0-3.6
<i>total</i>		707.9	0	$2.7_{\pm 0.75} \times 10^{-2}$	0-2.9	0-3.6
31.62	AL-NA	187.1	0	$< 1.8 \times 10^{-3} *$	0-2.9	0-3.6
	AL-EX	113.7	0	$< 1.8 \times 10^{-3}$	0-2.9	0-3.6
	AL-AU	73.6	0	$< 1.8 \times 10^{-3} *$	0-2.9	0-3.6
	EX-NI	70.2	0	$< 1.8 \times 10^{-3}$	0-2.9	0-3.6
	AL-EX-NA	57.8	0	$< 1.8 \times 10^{-4} *$	0-2.9	0-3.6
	EX-NA	52.9	0	$5_{-3.8}^{+3.4} \times 10^{-3}$	0-2.9	0-3.6
	AL-AU-EX	36.4	0	$< 1.8 \times 10^{-4} *$	0-2.9	0-3.6
	AL-AU-NA	24.7	0	$< 1.8 \times 10^{-4} *$	0-2.9	0-3.6
	AU-EX	17.2	0	$< 1.8 \times 10^{-3} *$	0-2.9	0-3.6
	AL-AU-EX-NA	14.2	0	—	0-2.9	0-3.6
	AL-NI	12.7	0	$< 1.8 \times 10^{-3} *$	0-2.9	0-3.6
	AL-AU-EX-NI	11.4	0	—	0-2.9	0-3.6
	AL-AU-NI	10.6	0	$< 1.8 \times 10^{-4} *$	0-2.9	0-3.6
	AU-EX-NI	10.1	0	$< 1.8 \times 10^{-4} *$	0-2.9	0-3.6

TABLE II. (*Continued*).

$H_t \times 10^{21}$ (Hz ⁻¹)	config	T_{obs} (days)	N_c	\bar{N}_b ^{5%} _{95%}	confidence interval	
					90%	95%
	AL-EX-NI	7.2	0	$< 1.8 \times 10^{-4} *$	0–2.9	0–3.6
	AU-NI	5.8	0	$< 1.8 \times 10^{-3} *$	0–2.9	0–3.6
	AU-NA	2.0	0	$< 1.8 \times 10^{-3} *$	0–2.9	0–3.6
	<i>total</i>	707.9	0	$2.1_{\pm 0.59} \times 10^{-2}$	0–2.9	0–3.6

TABLE III. Results of the event search analysis as described in the previous table but optimized for the galactic center direction (see Sec. III A).

$H_t \times 10^{21}$ (Hz ⁻¹)	config	T_{obs} (days)	N_c	\bar{N}_b ^{5%} _{95%}	confidence interval	
					90%	95%
2.24	AU-NA	1.6	0	$8.1_{-1.5}^{+1.5} \times 10^{-2}$	0–2.9	0–3.6
2.51	AU-NA	3.1	0	$0.1_{-0.017}^{+0.017}$	0–2.9	0–3.6
2.82	AL-NA	5.9	1	$0.9_{-0.05}^{+0.05}$	0–4	0–4.8
	AL-AU	5.0	0	$0.4_{-0.032}^{+0.032}$	0–2.9	0–3.6
	AU-NA	3.2	0	$0.2_{-0.025}^{+0.025}$	0–2.9	0–3.6
	<i>total</i>	14.0	1	1.5 ± 0.065	0–3.8	0–4.6
3.16	AL-NA	61.3	5	$3.6_{-0.099}^{+0.098}$	0–7	0–8.1
	AL-AU	36.3	1	$1.5_{-0.064}^{+0.063}$	0–3.8	0–4.6
	AL-AU-NA	4.5	0	—	0–2.9	0–3.6
	AL-EX	1.7	0	$0.2_{-0.024}^{+0.024}$	0–2.9	0–3.6
	AU-EX	1.2	0	$0.2_{-0.024}^{+0.024}$	0–2.9	0–3.6
	<i>total</i>	104.5	6	$5.5_{\pm 0.12}$	0–6.8	0–8
3.55	AL-NA	90.0	0	$1.4_{-0.063}^{+0.062}$	0–2.9	0–3.6
	AL-AU	54.5	0	$0.6_{-0.039}^{+0.039}$	0–2.9	0–3.6
	AL-AU-NA	9.7	0	$< 9.1 \times 10^{-4} *$	0–2.9	0–3.6
	AL-EX	5.1	0	$0.1_{-0.02}^{+0.02}$	0–2.9	0–3.6
	AU-EX	3.4	0	$0.4_{-0.033}^{+0.033}$	0–2.9	0–3.6
	EX-NI	2.0	2	$1.5_{-0.064}^{+0.063}$	0–4.9	0–5.8
	EX-NA	1.7	2	$0.5_{-0.038}^{+0.038}$	0–5.6	0–6.5
	AL-AU-EX	1.6	0	$< 9.1 \times 10^{-4}$	0–2.9	0–3.6
	<i>total</i>	167.6	4	$4.6_{\pm 0.11}$	0–5.4	0–6.5
	3.75	AL-NA	97.8	2	$1.0_{-0.053}^{+0.053}$	0–5.2
AL-AU		59.1	0	$0.3_{-0.029}^{+0.028}$	0–2.9	0–3.6
AL-AU-NA		10.9	0	$< 9.1 \times 10^{-4} *$	0–2.9	0–3.6
AL-EX		7.3	0	$5.7_{-1.3}^{+1.2} \times 10^{-2}$	0–2.9	0–3.6
AU-EX		4.9	0	$0.4_{-0.035}^{+0.035}$	0–2.9	0–3.6
EX-NI		3.5	1	$2.5_{-0.082}^{+0.082}$	0–3.6	0–4.4
AL-AU-EX		2.9	0	$< 9.1 \times 10^{-4} *$	0–2.9	0–3.6
EX-NA		2.3	0	$0.7_{-0.045}^{+0.044}$	0–2.9	0–3.6
AL-AU-EX-NA		1.8	0	—	0–2.9	0–3.6
AL-NI		1.6	0	$1.7_{-0.7}^{+0.65} \times 10^{-2}$	0–2.9	0–3.6
AU-NA		1.0	0	$2.5_{-0.84}^{+0.8} \times 10^{-2}$	0–2.9	0–3.6
<i>total</i>		192.8	3	$5.1_{\pm 0.12}$	0–4.4	0–5.4
3.98	AL-NA	105.1	3	$0.8_{-0.046}^{+0.046}$	0.0061–6.8	0–7.8
	AL-AU	59.6	0	$0.2_{-0.021}^{+0.02}$	0–2.9	0–3.6
	AL-AU-NA	12.2	0	$< 9.1 \times 10^{-4}$	0–2.9	0–3.6
	AL-EX	10.4	1	$9.2_{-1.6}^{+1.6} \times 10^{-2}$	0–4.5	0–5.3

TABLE III. (Continued).

$H_t \times 10^{21}$ (Hz ⁻¹)	config	T_{obs} (days)	N_c	\bar{N}_b ^{5%} _{95%}	confidence interval	
					90%	95%
	AU-EX	6.1	1	$0.3_{-0.03}^{+0.03}$	0–4.3	0–5.1
	EX-NI	6.0	6	$2.9_{-0.089}^{+0.089}$	0–8.7	0–10
	AL-AU-EX	4.4	0	$<9.1 \times 10^{-4}*$	0–2.9	0–3.6
	EX-NA	3.0	0	$0.7_{-0.044}^{+0.044}$	0–2.9	0–3.6
	AL-AU-EX-NA	2.8	0	—	0–2.9	0–3.6
	AL-NI	2.3	1	$3.5_{-0.99}^{+0.95} \times 10^{-2}$	0.014–4.6	0–5.4
	AL-AU-NI	1.9	0	—	0–2.9	0–3.6
	AL-AU-EX-NI	1.4	0	—	0–2.9	0–3.6
	AU-NA	1.1	0	$2.1_{-0.77}^{+0.73} \times 10^{-2}$	0–2.9	0–3.6
	<i>total</i>	215.8	12	$5.1_{\pm 0.12}$	1.5–15	0.88–16
4.47	AL-NA	116.9	0	$0.5_{-0.036}^{+0.036}$	0–2.9	0–3.6
	AL-AU	60.3	0	$8.6_{-1.5}^{+1.5} \times 10^{-2}$	0–2.9	0–3.6
	AL-EX	18.0	0	$8.5_{-1.5}^{+1.5} \times 10^{-2}$	0–2.9	0–3.6
	AL-AU-NA	14.4	0	$<9.1 \times 10^{-4}*$	0–2.9	0–3.6
	EX-NI	13.1	5	$4.1_{-0.11}^{+0.11}$	0–6.6	0–7.8
	AL-AU-EX	7.5	0	$<9.1 \times 10^{-4}*$	0–2.9	0–3.6
	AU-EX	7.5	0	$0.2_{-0.02}^{+0.02}$	0–2.9	0–3.6
	EX-NA	5.6	4	$3.0_{-0.09}^{+0.09}$	0–6.3	0–7.4
	AL-AU-EX-NA	5.1	0	—	0–2.9	0–3.6
	AL-AU-EX-NI	4.4	0	—	0–2.9	0–3.6
	AL-AU-NI	3.5	0	—	0–2.9	0–3.6
	AL-NI	3.2	0	$1.3_{-0.61}^{+0.57} \times 10^{-2}$	0–2.9	0–3.6
	AL-EX-NA	2.3	0	—	0–2.9	0–3.6
	AU-NI	1.7	0	$5.7_{-1.3}^{+1.2} \times 10^{-2}$	0–2.9	0–3.6
	AU-NA	1.2	0	$3.7_{-1}^{+0.98} \times 10^{-2}$	0–2.9	0–3.6
	<i>total</i>	264.7	9	$8_{\pm 0.15}$	0–8.1	0–9.4
5.01	AL-NA	125.3	0	$0.4_{-0.035}^{+0.034}$	0–2.9	0–3.6
	AL-AU	59.1	1	$6.4_{-1.3}^{+1.3} \times 10^{-2}$	0–4.5	0–5.4
	AL-EX	27.5	0	$7.9_{-1.5}^{+1.4} \times 10^{-2}$	0–2.9	0–3.6
	EX-NI	21.2	2	$4.2_{-0.11}^{+0.11}$	0–4	0–4.9
	AL-AU-NA	13.2	0	—	0–2.9	0–3.6
	EX-NA	9.8	10	$7.8_{-0.15}^{+0.15}$	0–9.2	0–11
	AL-AU-EX	9.7	0	—	0–2.9	0–3.6
	AU-EX	8.6	0	$0.2_{-0.023}^{+0.023}$	0–2.9	0–3.6
	AL-AU-EX-NA	7.3	0	—	0–2.9	0–3.6
	AL-AU-EX-NI	6.3	0	—	0–2.9	0–3.6
	AL-EX-NA	4.7	0	—	0–2.9	0–3.6
	AL-AU-NI	3.9	0	—	0–2.9	0–3.6
	AL-NI	3.0	0	$6_{-4.2}^{+3.8} \times 10^{-3}$	0–2.9	0–3.6
	AU-NI	2.5	1	$7.9_{-1.5}^{+1.4} \times 10^{-2}$	0–4.5	0–5.3
	AU-EX-NI	1.6	0	—	0–2.9	0–3.6
	AU-NA	1.3	0	$1.8_{-0.72}^{+0.67} \times 10^{-2}$	0–2.9	0–3.6
	<i>total</i>	306.8	14	$13_{\pm 0.19}$	0–9.6	0–11
5.62	AL-NA	130.8	0	$0.2_{-0.026}^{+0.025}$	0–2.9	0–3.6
	AL-AU	57.3	0	$3.9_{-1}^{+1} \times 10^{-2}$	0–2.9	0–3.6
	AL-EX	37.5	0	$0.1_{-0.018}^{+0.017}$	0–2.9	0–3.6
	EX-NI	29.4	6	$4.4_{-0.11}^{+0.11}$	0–7.5	0–8.7
	EX-NA	15.4	12	$10.5_{-0.17}^{+0.17}$	0–9.3	0–11
	AL-AU-NA	14.3	0	—	0–2.9	0–3.6

TABLE III. (*Continued*).

$H_t \times 10^{21}$ (Hz ⁻¹)	config	T_{obs} (days)	N_c	\bar{N}_b ^{5%} _{95%}	confidence interval	
					90%	95%
	AL-AU-EX	12.7	0	—	0–2.9	0–3.6
	AU-EX	9.6	0	$0.2^{+0.022}_{-0.022}$	0–2.9	0–3.6
	AL-AU-EX-NA	9.0	0	—	0–2.9	0–3.6
	AL-AU-EX-NI	8.3	0	—	0–2.9	0–3.6
	AL-EX-NA	8.3	0	—	0–2.9	0–3.6
	AL-NI	5.1	0	$4^{+3}_{-3.4} \times 10^{-3}$	0–2.9	0–3.6
	AL-AU-NI	4.5	0	—	0–2.9	0–3.6
	AU-NI	3.1	0	$2.6^{+0.82}_{-0.86} \times 10^{-2}$	0–2.9	0–3.6
	AU-EX-NI	2.4	0	—	0–2.9	0–3.6
	AL-EX-NI	1.5	0	—	0–2.9	0–3.6
	AU-NA	1.4	0	$8^{+4.4}_{-4.8} \times 10^{-3}$	0–2.9	0–3.6
	<i>total</i>	352.9	18	$16_{\pm 0.2}$	0–11	0–13
6.31	AL-NA	134.7	0	$0.2^{+0.026}_{-0.026}$	0–2.9	0–3.6
	AL-AU	55.6	0	$3.6^{+0.96}_{-1} \times 10^{-2}$	0–2.9	0–3.6
	AL-EX	48.0	0	$0.1^{+0.018}_{-0.018}$	0–2.9	0–3.6
	EX-NI	34.7	1	$2.9^{+0.088}_{-0.088}$	0–3.5	0–4.3
	EX-NA	20.9	8	$10.5^{+0.17}_{-0.17}$	0–6.1	0–7.3
	AL-AU-NA	15.2	0	—	0–2.9	0–3.6
	AL-AU-EX	15.1	0	—	0–2.9	0–3.6
	AL-EX-NA	12.4	0	—	0–2.9	0–3.6
	AL-AU-EX-NA	11.2	0	—	0–2.9	0–3.6
	AU-EX	10.2	0	$0.1^{+0.018}_{-0.018}$	0–2.9	0–3.6
	AL-AU-EX-NI	10.2	0	—	0–2.9	0–3.6
	AL-NI	6.7	0	$< 1.8 \times 10^{-3}$	0–2.9	0–3.6
	AL-AU-NI	5.3	0	—	0–2.9	0–3.6
	AU-NI	3.6	0	$1^{+0.5}_{-0.54} \times 10^{-2}$	0–2.9	0–3.6
	AU-EX-NI	3.3	0	—	0–2.9	0–3.6
	AL-EX-NI	2.3	0	—	0–2.9	0–3.6
	AU-NA	1.5	0	$< 1.8 \times 10^{-3}$	0–2.9	0–3.6
	<i>total</i>	392.8	9	$14_{\pm 0.19}$	0–5.6	0–6.8
7.08	AL-NA	137.5	0	$0.3^{+0.026}_{-0.027}$	0–2.9	0–3.6
	AL-EX	57.8	0	$0.1^{+0.019}_{-0.02}$	0–2.9	0–3.6
	AL-AU	54.8	0	$8^{+4.4}_{-4.8} \times 10^{-3}$	0–2.9	0–3.6
	EX-NI	39.5	3	$2.6^{+0.084}_{-0.085}$	0–5.4	0–6.4
	EX-NA	26.5	7	$10.3^{+0.17}_{-0.17}$	0–5.5	0–6.7
	AL-AU-EX	17.7	0	—	0–2.9	0–3.6
	AL-EX-NA	16.6	0	—	0–2.9	0–3.6
	AL-AU-NA	15.7	0	—	0–2.9	0–3.6
	AL-AU-EX-NA	12.6	0	—	0–2.9	0–3.6
	AL-AU-EX-NI	10.9	0	—	0–2.9	0–3.6
	AU-EX	10.9	0	$6.5^{+1.3}_{-1.3} \times 10^{-2}$	0–2.9	0–3.6
	AL-NI	7.5	0	$4^{+3}_{-3.4} \times 10^{-3}$	0–2.9	0–3.6
	AL-AU-NI	5.8	0	—	0–2.9	0–3.6
	AU-EX-NI	4.4	0	—	0–2.9	0–3.6
	AU-NI	3.5	0	$9^{+4.7}_{-5.1} \times 10^{-3}$	0–2.9	0–3.6
	AL-EX-NI	3.2	0	—	0–2.9	0–3.6
	AU-NA	1.4	0	$< 1.8 \times 10^{-3}$	0–2.9	0–3.6
	<i>total</i>	428.1	10	$13_{\pm 0.19}$	0–6.3	0–7.6
7.94	AL-NA	139.1	0	$0.2^{+0.023}_{-0.023}$	0–2.9	0–3.6
	AL-EX	67.2	0	$9.6^{+1.6}_{-1.6} \times 10^{-2}$	0–2.9	0–3.6

TABLE III. (Continued).

$H_t \times 10^{21}$ (Hz ⁻¹)	config	T_{obs} (days)	N_c	\bar{N}_b ^{5%} _{95%}	confidence interval	
					90%	95%
	AL-AU	54.3	0	$2_{-0.75}^{+0.71} \times 10^{-2}$	0–2.9	0–3.6
	EX-NI	43.4	4	$2.3_{-0.08}^{+0.079}$	0–6.7	0–7.8
	EX-NA	30.8	9	$6.2_{-0.13}^{+0.13}$	0–9.5	0–11
	AL-EX-NA	20.9	0	—	0–2.9	0–3.6
	AL-AU-EX	20.0	0	—	0–2.9	0–3.6
	AL-AU-NA	16.1	0	—	0–2.9	0–3.6
	AL-AU-EX-NA	13.6	0	—	0–2.9	0–3.6
	AU-EX	11.5	0	$6.3_{-1.3}^{+1.3} \times 10^{-2}$	0–2.9	0–3.6
	AL-AU-EX-NI	11.3	0	—	0–2.9	0–3.6
	AL-NI	8.0	0	$< 1.8 \times 10^{-3}$	0–2.9	0–3.6
	AL-AU-NI	6.1	0	—	0–2.9	0–3.6
	AU-EX-NI	5.1	0	—	0–2.9	0–3.6
	AL-EX-NI	3.9	0	—	0–2.9	0–3.6
	AU-NI	3.5	0	$< 1.8 \times 10^{-3}$	0–2.9	0–3.6
	AU-NA	1.4	0	$5_{-3.8}^{+3.4} \times 10^{-3}$	0–2.9	0–3.6
	<i>total</i>	458.2	13	$8.9_{\pm 0.16}$	0–12	0–13
8.91	AL-NA	141.2	0	$0.2_{-0.025}^{+0.025}$	0–2.9	0–3.6
	AL-EX	75.2	0	$0.1_{-0.018}^{+0.017}$	0–2.9	0–3.6
	AL-AU	55.1	0	$9_{-5.1}^{+4.7} \times 10^{-3}$	0–2.9	0–3.6
	EX-NI	46.7	2	$1.7_{-0.068}^{+0.068}$	0–4.8	0–5.7
	EX-NA	33.5	5	$3.8_{-0.1}^{+0.1}$	0–6.8	0–8
	AL-EX-NA	24.9	0	—	0–2.9	0–3.6
	AL-AU-EX	21.9	0	—	0–2.9	0–3.6
	AL-AU-NA	16.5	0	—	0–2.9	0–3.6
	AL-AU-EX-NA	14.1	0	—	0–2.9	0–3.6
	AU-EX	12.0	0	$4.5_{-1.1}^{+1.1} \times 10^{-2}$	0–2.9	0–3.6
	AL-AU-EX-NI	11.4	0	—	0–2.9	0–3.6
	AL-NI	8.4	0	$3_{-3}^{+2.6} \times 10^{-3}$	0–2.9	0–3.6
	AL-AU-NI	6.4	0	—	0–2.9	0–3.6
	AU-EX-NI	5.7	0	—	0–2.9	0–3.6
	AL-EX-NI	4.4	0	—	0–2.9	0–3.6
	AU-NI	3.7	0	$8_{-4.8}^{+4.4} \times 10^{-3}$	0–2.9	0–3.6
	AU-NA	1.4	0	$< 3.4 \times 10^{-3}$	0–2.9	0–3.6
	<i>total</i>	485.0	7	$5.9_{\pm 0.13}$	0–7.5	0–8.8
10.00	AL-NA	144.0	0	$0.1_{-0.018}^{+0.018}$	0–2.9	0–3.6
	AL-EX	81.2	0	$0.1_{-0.017}^{+0.016}$	0–2.9	0–3.6
	AL-AU	56.0	0	$1.4_{-0.63}^{+0.59} \times 10^{-2}$	0–2.9	0–3.6
	EX-NI	49.3	1	$1.5_{-0.064}^{+0.064}$	0–3.8	0–4.6
	EX-NA	35.6	2	$3.0_{-0.09}^{+0.089}$	0–4.3	0–5.2
	AL-EX-NA	28.0	0	—	0–2.9	0–3.6
	AL-AU-EX	23.0	0	—	0–2.9	0–3.6
	AL-AU-NA	16.9	0	—	0–2.9	0–3.6
	AL-AU-EX-NA	14.2	0	—	0–2.9	0–3.6
	AU-EX	12.6	0	$5.5_{-1.2}^{+1.2} \times 10^{-2}$	0–2.9	0–3.6
	AL-AU-EX-NI	11.4	0	—	0–2.9	0–3.6
	AL-NI	8.8	0	$4_{-3.4}^{+3} \times 10^{-3}$	0–2.9	0–3.6
	AL-AU-NI	6.6	0	—	0–2.9	0–3.6
	AU-EX-NI	6.1	0	—	0–2.9	0–3.6
	AL-EX-NI	4.9	0	—	0–2.9	0–3.6
	AU-NI	3.8	0	$5_{-3.8}^{+3.4} \times 10^{-3}$	0–2.9	0–3.6

TABLE III. (*Continued*).

$H_t \times 10^{21}$ (Hz ⁻¹)	config	T_{obs} (days)	N_c	\bar{N}_b ^{5%} _{95%}	confidence interval	
					90%	95%
	AU-NA	1.5	0	$<1.8 \times 10^{-3}$	0–2.9	0–3.6
	<i>total</i>	506.7	3	$4.8_{\pm 0.11}$	0–4.5	0–5.5
11.22	AL-NA	146.8	0	$0.1^{+0.019}_{-0.02}$	0–2.9	0–3.6
	AL-EX	85.0	0	$5.2^{+1.2}_{-1.2} \times 10^{-2}$	0–2.9	0–3.6
	AL-AU	57.2	0	$1.8^{+0.67}_{-0.72} \times 10^{-2}$	0–2.9	0–3.6
	EX-NI	51.4	0	$1.3^{+0.06}_{-0.06}$	0–2.9	0–3.6
	EX-NA	37.1	3	$2.6^{+0.084}_{-0.084}$	0–5.4	0–6.4
	AL-EX-NA	30.6	0	—	0–2.9	0–3.6
	AL-AU-EX	24.0	0	—	0–2.9	0–3.6
	AL-AU-NA	17.3	0	—	0–2.9	0–3.6
	AL-AU-EX-NA	14.2	0	—	0–2.9	0–3.6
	AU-EX	12.9	0	$3.8^{+0.99}_{-1} \times 10^{-2}$	0–2.9	0–3.6
	AL-AU-EX-NI	11.4	0	—	0–2.9	0–3.6
	AL-NI	9.2	0	$3^{+2.6}_{-3} \times 10^{-3}$	0–2.9	0–3.6
	AL-AU-NI	6.8	0	—	0–2.9	0–3.6
	AU-EX-NI	6.5	0	—	0–2.9	0–3.6
	AL-EX-NI	5.2	0	—	0–2.9	0–3.6
	AU-NI	3.9	0	$4^{+3}_{-3.4} \times 10^{-3}$	0–2.9	0–3.6
	AU-NA	1.5	0	$<1.8 \times 10^{-3}$	0–2.9	0–3.6
	<i>total</i>	523.3	3	$4.2_{\pm 0.11}$	0–4.7	0–5.7
12.59	AL-NA	149.3	0	$0.2^{+0.021}_{-0.022}$	0–2.9	0–3.6
	AL-EX	87.7	0	$9.7^{+1.6}_{-1.6} \times 10^{-2}$	0–2.9	0–3.6
	AL-AU	58.3	0	$1.4^{+0.59}_{-0.63} \times 10^{-2}$	0–2.9	0–3.6
	EX-NI	53.0	3	$1.1^{+0.055}_{-0.055}$	0–6.5	0–7.5
	EX-NA	38.3	1	$1.8^{+0.07}_{-0.071}$	0–3.7	0–4.5
	AL-EX-NA	32.7	0	—	0–2.9	0–3.6
	AL-AU-EX	24.6	0	—	0–2.9	0–3.6
	AL-AU-NA	17.5	0	—	0–2.9	0–3.6
	AL-AU-EX-NA	14.2	0	—	0–2.9	0–3.6
	AU-EX	13.2	0	$2.8^{+0.85}_{-0.89} \times 10^{-2}$	0–2.9	0–3.6
	AL-AU-EX-NI	11.4	0	—	0–2.9	0–3.6
	AL-NI	9.5	0	$<1.8 \times 10^{-3}$	0–2.9	0–3.6
	AL-AU-NI	7.0	0	—	0–2.9	0–3.6
	AU-EX-NI	6.7	0	—	0–2.9	0–3.6
	AL-EX-NI	5.3	0	—	0–2.9	0–3.6
	AU-NI	4.1	0	$<1.8 \times 10^{-3}$	0–2.9	0–3.6
	AU-NA	1.6	0	$<1.8 \times 10^{-3}$	0–2.9	0–3.6
	<i>total</i>	536.4	4	$3.3_{\pm 0.094}$	0–6.1	0–7.2
14.12	AL-NA	151.6	0	$0.1^{+0.017}_{-0.017}$	0–2.9	0–3.6
	AL-EX	89.7	0	$7.5^{+1.4}_{-1.4} \times 10^{-2}$	0–2.9	0–3.6
	AL-AU	59.3	0	$9^{+4.7}_{-5.1} \times 10^{-3}$	0–2.9	0–3.6
	EX-NI	54.4	2	$0.9^{+0.048}_{-0.048}$	0–5.3	0–6.3
	EX-NA	39.4	1	$1.7^{+0.067}_{-0.068}$	0–3.7	0–4.5
	AL-EX-NA	34.4	0	—	0–2.9	0–3.6
	AL-AU-EX	25.2	0	—	0–2.9	0–3.6
	AL-AU-NA	17.8	0	—	0–2.9	0–3.6
	AL-AU-EX-NA	14.2	0	—	0–2.9	0–3.6
	AU-EX	13.5	0	$4.3^{+1.1}_{-1.1} \times 10^{-2}$	0–2.9	0–3.6
	AL-AU-EX-NI	11.4	0	—	0–2.9	0–3.6
	AL-NI	9.8	0	$<1.8 \times 10^{-3}$	0–2.9	0–3.6

TABLE III. (Continued).

$H_t \times 10^{21}$ (Hz ⁻¹)	config	T_{obs} (days)	N_c	\bar{N}_b ^{5%} _{95%}	confidence interval	
					90%	95%
	AL-AU-NI	7.2	0	—	0–2.9	0–3.6
	AU-EX-NI	6.9	0	—	0–2.9	0–3.6
	AL-EX-NI	5.5	0	—	0–2.9	0–3.6
	AU-NI	4.2	0	$3_{-3}^{+2.6} \times 10^{-3}$	0–2.9	0–3.6
	AU-NA	1.6	0	$7_{-4.5}^{+4.1} \times 10^{-3}$	0–2.9	0–3.6
	<i>total</i>	547.5	3	$2.8_{\pm 0.087}$	0–5.3	0–6.3
15.85	AL-NA	153.7	1	$0.1_{-0.019}^{+0.018}$	0–4.5	0–5.3
	AL-EX	91.4	0	$4.8_{-1.2}^{+1.1} \times 10^{-2}$	0–2.9	0–3.6
	AL-AU	60.2	0	$6_{-4.2}^{+3.8} \times 10^{-3}$	0–2.9	0–3.6
	EX-NI	55.9	0	$0.9_{-0.049}^{+0.049}$	0–2.9	0–3.6
	EX-NA	40.3	1	$1.3_{-0.06}^{+0.06}$	0–3.8	0–4.7
	AL-EX-NA	35.7	0	—	0–2.9	0–3.6
	AL-AU-EX	25.7	0	—	0–2.9	0–3.6
	AL-AU-NA	18.0	0	—	0–2.9	0–3.6
	AL-AU-EX-NA	14.2	0	—	0–2.9	0–3.6
	AU-EX	13.7	0	$3.2_{-0.95}^{+0.91} \times 10^{-2}$	0–2.9	0–3.6
	AL-AU-EX-NI	11.4	0	—	0–2.9	0–3.6
	AL-NI	10.1	0	$< 1.8 \times 10^{-3}$	0–2.9	0–3.6
	AL-AU-NI	7.4	0	—	0–2.9	0–3.6
	AU-EX-NI	7.1	0	—	0–2.9	0–3.6
	AL-EX-NI	5.6	0	—	0–2.9	0–3.6
	AU-NI	4.3	0	$3_{-3}^{+2.6} \times 10^{-3}$	0–2.9	0–3.6
	AU-NA	1.6	0	$< 1.8 \times 10^{-3}$ *	0–2.9	0–3.6
	<i>total</i>	557.5	2	$2.4_{\pm 0.081}$	0–4.5	0–5.4
17.78	AL-NA	155.7	0	$0.1_{-0.019}^{+0.018}$	0–2.9	0–3.6
	AL-EX	93.0	0	$4.3_{-1.1}^{+1.1} \times 10^{-2}$	0–2.9	0–3.6
	AL-AU	61.0	0	$< 1.8 \times 10^{-3}$	0–2.9	0–3.6
	EX-NI	57.0	0	$0.8_{-0.047}^{+0.047}$	0–2.9	0–3.6
	EX-NA	41.2	1	$1.1_{-0.054}^{+0.053}$	0–3.9	0–4.8
	AL-EX-NA	36.7	0	—	0–2.9	0–3.6
	AL-AU-EX	26.1	0	—	0–2.9	0–3.6
	AL-AU-NA	18.3	0	—	0–2.9	0–3.6
	AL-AU-EX-NA	14.2	0	—	0–2.9	0–3.6
	AU-EX	13.8	0	$2.6_{-0.86}^{+0.82} \times 10^{-2}$	0–2.9	0–3.6
	AL-AU-EX-NI	11.4	0	—	0–2.9	0–3.6
	AL-NI	10.4	0	$< 1.8 \times 10^{-3}$	0–2.9	0–3.6
	AL-AU-NI	7.6	0	—	0–2.9	0–3.6
	AU-EX-NI	7.2	0	—	0–2.9	0–3.6
	AL-EX-NI	5.7	0	—	0–2.9	0–3.6
	AU-NI	4.5	0	$< 3.4 \times 10^{-3}$	0–2.9	0–3.6
	AU-NA	1.7	0	$< 3.4 \times 10^{-3}$	0–2.9	0–3.6
	<i>total</i>	566.6	1	$2.1_{\pm 0.075}$	0–3.6	0–4.5
19.95	AL-NA	157.6	1	$0.1_{-0.017}^{+0.017}$	0–4.5	0–5.3
	AL-EX	94.4	0	$4.2_{-1.1}^{+1} \times 10^{-2}$	0–2.9	0–3.6
	AL-AU	61.8	0	$5_{-3.8}^{+3.4} \times 10^{-3}$	0–2.9	0–3.6
	EX-NI	58.1	1	$0.8_{-0.046}^{+0.045}$	0–4.1	0–4.9
	EX-NA	41.9	0	$1.0_{-0.052}^{+0.052}$	0–2.9	0–3.6
	AL-EX-NA	37.5	0	—	0–2.9	0–3.6
	AL-AU-EX	26.5	0	—	0–2.9	0–3.6
	AL-AU-NA	18.5	0	—	0–2.9	0–3.6

TABLE III. (*Continued*).

$H_t \times 10^{21}$ (Hz ⁻¹)	config	T_{obs} (days)	N_c	\bar{N}_b ^{5%} _{95%}	confidence interval	
					90%	95%
	AL-AU-EX-NA	14.2	0	—	0–2.9	0–3.6
	AU-EX	14.0	0	$1.1^{+0.52}_{-0.56} \times 10^{-2}$	0–2.9	0–3.6
	AL-AU-EX-NI	11.4	0	—	0–2.9	0–3.6
	AL-NI	10.7	0	$9^{+4.7}_{-5.1} \times 10^{-3}$	0–2.9	0–3.6
	AL-AU-NI	7.7	0	—	0–2.9	0–3.6
	AU-EX-NI	7.3	0	—	0–2.9	0–3.6
	AL-EX-NI	5.8	0	—	0–2.9	0–3.6
	AU-NI	4.6	0	$4^{+3}_{-3.4} \times 10^{-3}$	0–2.9	0–3.6
	AU-NA	1.7	0	$<1.8 \times 10^{-3}$ *	0–2.9	0–3.6
	<i>total</i>	574.8	2	$1.9_{\pm 0.072}$	0–4.7	0–5.6
22.39	AL-NA	159.3	0	$4.8^{+1.1}_{-1.2} \times 10^{-2}$	0–2.9	0–3.6
	AL-EX	95.7	0	$7.1^{+1.4}_{-1.4} \times 10^{-2}$	0–2.9	0–3.6
	AL-AU	62.5	0	$<3.4 \times 10^{-3}$	0–2.9	0–3.6
	EX-NI	59.0	2	$0.6^{+0.04}_{-0.041}$	0–5.5	0–6.5
	EX-NA	42.7	1	$1.0^{+0.052}_{-0.053}$	0–3.9	0–4.8
	AL-EX-NA	38.3	0	—	0–2.9	0–3.6
	AL-AU-EX	26.9	0	—	0–2.9	0–3.6
	AL-AU-NA	18.7	0	—	0–2.9	0–3.6
	AL-AU-EX-NA	14.2	0	—	0–2.9	0–3.6
	AU-EX	14.2	0	$3.5^{+0.95}_{-0.99} \times 10^{-2}$	0–2.9	0–3.6
	AL-AU-EX-NI	11.4	0	—	0–2.9	0–3.6
	AL-NI	11.1	0	$<1.8 \times 10^{-3}$	0–2.9	0–3.6
	AL-AU-NI	7.8	0	—	0–2.9	0–3.6
	AU-EX-NI	7.4	0	—	0–2.9	0–3.6
	AL-EX-NI	5.9	0	—	0–2.9	0–3.6
	AU-NI	4.7	0	$9^{+4.7}_{-5.1} \times 10^{-3}$	0–2.9	0–3.6
	AU-NA	1.7	0	$<1.8 \times 10^{-3}$ *	0–2.9	0–3.6
	<i>total</i>	582.6	3	$1.8_{\pm 0.07}$	0–5.9	0–6.9
25.12	AL-NA	161.0	0	$7.8^{+1.4}_{-1.5} \times 10^{-2}$	0–2.9	0–3.6
	AL-EX	96.9	0	$7.1^{+1.4}_{-1.4} \times 10^{-2}$	0–2.9	0–3.6
	AL-AU	63.2	0	$6^{+3.8}_{-4.2} \times 10^{-3}$	0–2.9	0–3.6
	EX-NI	59.7	1	$0.5^{+0.035}_{-0.035}$	0–4.2	0–5.1
	EX-NA	43.3	0	$1.0^{+0.052}_{-0.053}$	0–2.9	0–3.6
	AL-EX-NA	39.0	0	—	0–2.9	0–3.6
	AL-AU-EX	27.2	0	—	0–2.9	0–3.6
	AL-AU-NA	18.9	0	—	0–2.9	0–3.6
	AU-EX	14.4	0	$2.7^{+0.83}_{-0.87} \times 10^{-2}$	0–2.9	0–3.6
	AL-AU-EX-NA	14.2	0	—	0–2.9	0–3.6
	AL-AU-EX-NI	11.4	0	—	0–2.9	0–3.6
	AL-NI	11.4	0	$<1.8 \times 10^{-3}$ *	0–2.9	0–3.6
	AL-AU-NI	7.9	0	—	0–2.9	0–3.6
	AU-EX-NI	7.5	0	—	0–2.9	0–3.6
	AL-EX-NI	6.0	0	—	0–2.9	0–3.6
	AU-NI	4.8	0	$4^{+3}_{-3.4} \times 10^{-3}$	0–2.9	0–3.6
	AU-NA	1.7	0	$<1.8 \times 10^{-3}$ *	0–2.9	0–3.6
	<i>total</i>	589.7	1	$1.7_{\pm 0.067}$	0–3.7	0–4.6
28.18	AL-NA	162.6	0	$0.1^{+0.017}_{-0.018}$	0–2.9	0–3.6
	AL-EX	98.0	0	$6.6^{+1.3}_{-1.4} \times 10^{-2}$	0–2.9	0–3.6
	AL-AU	63.8	0	$3^{+2.6}_{-3} \times 10^{-3}$	0–2.9	0–3.6
	EX-NI	60.3	1	$0.3^{+0.027}_{-0.028}$	0–4.3	0–5.2

TABLE III. (Continued).

$H_t \times 10^{21}$ (Hz^{-1})	config	T_{obs} (days)	N_c	\bar{N}_b $^{5\%}_{95\%}$	confidence interval	
					90%	95%
	EX-NA	43.9	0	$0.9^{+0.05}_{-0.05}$	0–2.9	0–3.6
	AL-EX-NA	39.6	0	—	0–2.9	0–3.6
	AL-AU-EX	27.5	0	—	0–2.9	0–3.6
	AL-AU-NA	19.1	0	—	0–2.9	0–3.6
	AU-EX	14.6	0	$1.3^{+0.57}_{-0.61} \times 10^{-2}$	0–2.9	0–3.6
	AL-AU-EX-NA	14.2	0	—	0–2.9	0–3.6
	AL-NI	11.6	0	$< 3.4 \times 10^{-3}$	0–2.9	0–3.6
	AL-AU-EX-NI	11.4	0	—	0–2.9	0–3.6
	AL-AU-NI	7.9	0	—	0–2.9	0–3.6
	AU-EX-NI	7.6	0	—	0–2.9	0–3.6
	AL-EX-NI	6.0	0	—	0–2.9	0–3.6
	AU-NI	4.9	0	$< 3.4 \times 10^{-3}$	0–2.9	0–3.6
	AU-NA	1.7	0	$< 1.8 \times 10^{-3}*$	0–2.9	0–3.6
	<i>total</i>	596.1	1	$1.4_{\pm 0.061}$	0–3.8	0–4.6
31.62	AL-NA	164.1	0	$5.6^{+1.2}_{-1.3} \times 10^{-2}$	0–2.9	0–3.6
	AL-EX	99.0	0	$7.4^{+1.4}_{-1.4} \times 10^{-2}$	0–2.9	0–3.6
	AL-AU	64.5	0	$3^{+2.6}_{-3} \times 10^{-3}$	0–2.9	0–3.6
	EX-NI	60.9	1	$0.2^{+0.024}_{-0.024}$	0–4.4	0–5.2
	EX-NA	44.4	1	$0.8^{+0.047}_{-0.047}$	0–4	0–4.9
	AL-EX-NA	40.2	0	—	0–2.9	0–3.6
	AL-AU-EX	27.8	0	—	0–2.9	0–3.6
	AL-AU-NA	19.2	0	—	0–2.9	0–3.6
	AU-EX	14.7	0	$2.1^{+0.73}_{-0.77} \times 10^{-2}$	0–2.9	0–3.6
	AL-AU-EX-NA	14.2	0	—	0–2.9	0–3.6
	AL-NI	11.7	0	$< 1.8 \times 10^{-3}$	0–2.9	0–3.6
	AL-AU-EX-NI	11.4	0	—	0–2.9	0–3.6
	AL-AU-NI	8.0	0	—	0–2.9	0–3.6
	AU-EX-NI	7.7	0	—	0–2.9	0–3.6
	AL-EX-NI	6.1	0	—	0–2.9	0–3.6
	AU-NI	5.0	0	$4^{+3}_{-3.4} \times 10^{-3}$	0–2.9	0–3.6
	AU-NA	1.7	0	$4^{+3}_{-3.4} \times 10^{-3}$	0–2.9	0–3.6
	<i>total</i>	602.1	2	$1.2_{\pm 0.057}$	0–5.1	0–6
35.48	AL-NA	165.6	0	$0.1^{+0.018}_{-0.019}$	0–2.9	0–3.6
	AL-EX	99.9	0	$4.6^{+1.1}_{-1.1} \times 10^{-2}$	0–2.9	0–3.6
	AL-AU	65.1	0	$9^{+4.7}_{-5.1} \times 10^{-3}$	0–2.9	0–3.6
	EX-NI	61.5	0	$0.2^{+0.022}_{-0.022}$	0–2.9	0–3.6
	EX-NA	45.0	0	$0.8^{+0.046}_{-0.046}$	0–2.9	0–3.6
	AL-EX-NA	40.8	0	—	0–2.9	0–3.6
	AL-AU-EX	28.1	0	—	0–2.9	0–3.6
	AL-AU-NA	19.4	0	—	0–2.9	0–3.6
	AU-EX	14.9	0	$2.8^{+0.85}_{-0.89} \times 10^{-2}$	0–2.9	0–3.6
	AL-AU-EX-NA	14.2	0	—	0–2.9	0–3.6
	AL-NI	11.8	0	$< 1.8 \times 10^{-3}*$	0–2.9	0–3.6
	AL-AU-EX-NI	11.4	0	—	0–2.9	0–3.6
	AL-AU-NI	8.1	0	—	0–2.9	0–3.6
	AU-EX-NI	7.8	0	—	0–2.9	0–3.6
	AL-EX-NI	6.1	0	—	0–2.9	0–3.6
	AU-NI	5.0	0	$3^{+2.6}_{-3} \times 10^{-3}$	0–2.9	0–3.6
	AU-NA	1.8	0	$< 1.8 \times 10^{-3}*$	0–2.9	0–3.6
	<i>total</i>	607.8	0	$1.2_{\pm 0.057}$	0–2.9	0–3.6

TABLE III. (*Continued*).

$H_t \times 10^{21}$ (Hz ⁻¹)	config	T_{obs} (days)	N_c	\bar{N}_b ^{5%} _{95%}	confidence interval	
					90%	95%
	EX-NA	45.5	1	$0.6^{+0.04}_{-0.041}$	0-4.1	0-5
	AL-EX-NA	41.4	0	—	0-2.9	0-3.6
	AL-AU-EX	28.3	0	—	0-2.9	0-3.6
	AL-AU-NA	19.6	0	—	0-2.9	0-3.6
	AU-EX	15.0	0	$3.2^{+0.91}_{-0.95} \times 10^{-2}$	0-2.9	0-3.6
	AL-AU-EX-NA	14.2	0	—	0-2.9	0-3.6
	AL-NI	11.9	0	$3^{+2.6}_{-3} \times 10^{-3}$	0-2.9	0-3.6
	AL-AU-EX-NI	11.4	0	—	0-2.9	0-3.6
	AL-AU-NI	8.2	0	—	0-2.9	0-3.6
	AU-EX-NI	7.9	0	—	0-2.9	0-3.6
	AL-EX-NI	6.2	0	—	0-2.9	0-3.6
	AU-NI	5.1	0	$3^{+2.6}_{-3} \times 10^{-3}$	0-2.9	0-3.6
	AU-NA	1.8	0	$< 1.8 \times 10^{-3}*$	0-2.9	0-3.6
	<i>total</i>	613.3	1	$0.9_{\pm 0.049}$	0-4	0-4.8
44.67	AL-NA	168.5	0	$0.1^{+0.018}_{-0.018}$	0-2.9	0-3.6
	AL-EX	101.7	0	$1.5^{+0.61}_{-0.66} \times 10^{-2}$	0-2.9	0-3.6
	AL-AU	66.3	0	$< 1.8 \times 10^{-3}$	0-2.9	0-3.6
	EX-NI	62.5	0	$8.8^{+1.5}_{-1.6} \times 10^{-2}$	0-2.9	0-3.6
	EX-NA	45.9	0	$0.7^{+0.043}_{-0.043}$	0-2.9	0-3.6
	AL-EX-NA	42.0	0	—	0-2.9	0-3.6
	AL-AU-EX	28.6	0	—	0-2.9	0-3.6
	AL-AU-NA	19.7	0	—	0-2.9	0-3.6
	AU-EX	15.1	0	$1.8^{+0.67}_{-0.72} \times 10^{-2}$	0-2.9	0-3.6
	AL-AU-EX-NA	14.2	0	—	0-2.9	0-3.6
	AL-NI	12.0	0	$< 1.8 \times 10^{-3}$	0-2.9	0-3.6
	AL-AU-EX-NI	11.4	0	—	0-2.9	0-3.6
	AL-AU-NI	8.3	0	—	0-2.9	0-3.6
	AU-EX-NI	8.0	0	—	0-2.9	0-3.6
	AL-EX-NI	6.2	0	—	0-2.9	0-3.6
	AU-NI	5.1	0	$< 3.4 \times 10^{-3}$	0-2.9	0-3.6
	AU-NA	1.8	0	$< 1.8 \times 10^{-3}*$	0-2.9	0-3.6
	<i>total</i>	618.6	0	$0.93_{\pm 0.05}$	0-2.9	0-3.6
50.12	AL-NA	169.9	0	$0.3^{+0.026}_{-0.027}$	0-2.9	0-3.6
	AL-EX	102.5	0	$4.2^{+1}_{-1.1} \times 10^{-2}$	0-2.9	0-3.6
	AL-AU	66.9	0	$2.2^{+0.75}_{-0.79} \times 10^{-2}$	0-2.9	0-3.6
	EX-NI	63.0	0	$6.9^{+1.3}_{-1.4} \times 10^{-2}$	0-2.9	0-3.6
	EX-NA	46.4	0	$0.6^{+0.039}_{-0.039}$	0-2.9	0-3.6
	AL-EX-NA	42.5	0	—	0-2.9	0-3.6
	AL-AU-EX	28.8	0	—	0-2.9	0-3.6
	AL-AU-NA	19.9	0	—	0-2.9	0-3.6
	AU-EX	15.2	0	$4^{+3}_{-3.4} \times 10^{-3}$	0-2.9	0-3.6
	AL-AU-EX-NA	14.2	0	—	0-2.9	0-3.6
	AL-NI	12.2	0	$< 1.8 \times 10^{-3}*$	0-2.9	0-3.6
	AL-AU-EX-NI	11.4	0	—	0-2.9	0-3.6
	AL-AU-NI	8.3	0	—	0-2.9	0-3.6
	AU-EX-NI	8.1	0	—	0-2.9	0-3.6
	AL-EX-NI	6.3	0	—	0-2.9	0-3.6
	AU-NI	5.2	0	$< 1.8 \times 10^{-3}$	0-2.9	0-3.6
	AU-NA	1.8	0	$< 1.8 \times 10^{-3}*$	0-2.9	0-3.6
	<i>total</i>	623.7	0	$0.96_{\pm 0.051}$	0-2.9	0-3.6

TABLE III. (Continued).

$H_t \times 10^{21}$ (Hz^{-1})	config	T_{obs} (days)	N_c	\bar{N}_b $^{5\%}_{95\%}$	confidence interval		
					90%	95%	
56.23	AL-NA	171.4	1	$0.1^{+0.017}_{-0.018}$	0–4.5	0–5.3	
	AL-EX	103.2	0	$2.8^{+0.85}_{-0.89} \times 10^{-2}$	0–2.9	0–3.6	
	AL-AU	67.5	0	$1.1^{+0.52}_{-0.56} \times 10^{-2}$	0–2.9	0–3.6	
	EX-NI	63.5	0	$4.8^{+1.1}_{-1.2} \times 10^{-2}$	0–2.9	0–3.6	
	EX-NA	46.8	0	$0.6^{+0.038}_{-0.039}$	0–2.9	0–3.6	
	AL-EX-NA	43.0	0	—	0–2.9	0–3.6	
	AL-AU-EX	29.1	0	—	0–2.9	0–3.6	
	AL-AU-NA	20.0	0	—	0–2.9	0–3.6	
	AU-EX	15.3	0	$1.4^{+0.59}_{-0.63} \times 10^{-2}$	0–2.9	0–3.6	
	AL-AU-EX-NA	14.2	0	—	0–2.9	0–3.6	
	AL-NI	12.3	0	$< 1.8 \times 10^{-3}*$	0–2.9	0–3.6	
	AL-AU-EX-NI	11.4	0	—	0–2.9	0–3.6	
	AL-AU-NI	8.4	0	—	0–2.9	0–3.6	
	AU-EX-NI	8.1	0	—	0–2.9	0–3.6	
	AL-EX-NI	6.3	0	—	0–2.9	0–3.6	
	AU-NI	5.2	0	$< 1.8 \times 10^{-3}$	0–2.9	0–3.6	
	AU-NA	1.8	0	$< 1.8 \times 10^{-3}*$	0–2.9	0–3.6	
	<i>total</i>		628.6	1	$0.77_{\pm 0.046}$	0–4.1	0–4.9

- [1] E. Mauceli, Z. K. Geng, W. O. Hamilton, W. W. Johnson, S. Merkowitz, A. Morse, B. Price, and N. Solomonson, *Phys. Rev. Lett.* **54**, 1264 (1996).
- [2] G. A. Prodi *et al.*, in *Gravitational Waves—Proceedings of the 2nd Edoardo Amaldi Conference On Gravitational Waves*, edited by E. Cocchia, G. Veneziano, and P. G. Pizzella (World Scientific, Singapore, 1999), p. 148.
- [3] P. Astone *et al.*, *Phys. Rev. D* **47**, 362 (1993); from 1998 Explorer is a CERN Recognized Experiment.
- [4] P. Astone *et al.*, *Astropart. Phys.* **7**, 231 (1997).
- [5] D. G. Blair, E. N. Ivanov, M. E. Tobar, P. J. Turner, F. van Kann, and I. S. Heng, *Phys. Rev. Lett.* **74**, 1908 (1995).
- [6] J. Baker, M. Campanelli, C. O. Lousto, and R. Takahashi, *Phys. Rev. D* **65**, 124012 (2002).
- [7] K. Belczynski, V. Kalogera, and T. Bulik, *Astrophys. J.* **572**, 407 (2001).
- [8] E. Amaldi *et al.*, *Astron. Astrophys.* **216**, 325 (1989).
- [9] P. Astone *et al.*, *Phys. Rev. D* **59**, 122001 (1999).
- [10] P. Astone *et al.*, *Astropart. Phys.* **10**, 83 (1999).
- [11] P. Astone *et al.*, *Class. Quantum Grav.* **18**, 243 (2001).
- [12] Z. A. Allen *et al.*, *Phys. Rev. Lett.* **85**, 5046 (2000).
- [13] P. Astone *et al.*, *Class. Quantum Grav.* **19**, 1367 (2002).
- [14] R. McDonough and A. Whalen, *Detection of Signals in Noise*, 2nd ed. (Academic, New York, 1995).
- [15] P. Astone, C. Buttiglione, S. Frasca, G. V. Pallottino, and G. Pizzella, *Nuovo Cimento Soc. Ital. Fis., C* **20**, 9 (1997).
- [16] L. Baggio *et al.*, *Phys. Rev. D* **61**, 102001 (2000).
- [17] G. A. Prodi, L. Baggio, M. Cerdonio, V. Crivelli Visconti, V. Martinucci, A. Ortolan, L. Taffarello, G. Vedovato, S. Vitale, and J. Zendri, in *Gravitational Waves—Proceedings of the 3rd Edoardo Amaldi Conference On Gravitational Waves*, edited by S. Meshkov, AIP Conf. Proc. No. 523 (AIP, Melville, NY, 2000), p. 148.
- [18] A. Ortolan, L. Baggio, M. Cerdonio, I. S. Heng, G. A. Prodi, G. Vedovato, and S. Vitale, *Class. Quantum Grav.* **19**, 1457 (2002).
- [19] G. A. Prodi *et al.*, *Int. J. Mod. Phys. D* **9**, 237 (2000).
- [20] P. Astone, S. D. Antonio, and G. Pizzella, *Phys. Rev. D* **62**, 042001 (2000).
- [21] L. Baggio, M. Cerdonio, I. S. Heng, A. Ortolan, G. A. Prodi, E. Rocco, G. Vedovato, and S. Vitale, *Class. Quantum Grav.* **19**, 1541 (2002).
- [22] I. S. Heng, D. G. Blair, E. N. Ivanov, and M. E. Tobar, *Phys. Lett. A* **218**, 190 (1996).
- [23] L. Baggio *et al.*, *Nucl. Phys. B (Proc. Suppl.)* **70**, 357 (1999).
- [24] G. J. Feldman and R. D. Cousins, *Phys. Rev. D* **57**, 3873 (1998).
- [25] B. P. Roe and M. B. Woodroffe, *Phys. Rev. D* **63**, 013009 (2000).
- [26] P. Astone *et al.*, *Class. Quantum Grav.* **19**, 5449 (2002).
- [27] P. Astone *et al.*, *Class. Quantum Grav.* **19**, 1905 (2002).
- [28] J.-P. Zendri *et al.*, *Class. Quantum Grav.* **19**, 1925 (2002).
- [29] A. Papoulis, *Probability, Random Variables and Stochastic Processes*, 2nd ed. (McGraw Hill, New York, 1984), p. 115.
- [30] L. Baggio *et al.* (in preparation).
- [31] I. S. Heng, P. Bonifazi, D. G. Blair, E. N. Ivanov, and M. E. Tobar, *Gen. Relativ. Gravit.* **32**, 1281 (2000).